

The *HST* Survey of BL Lacertae Objects. I. Surface Brightness Profiles, Magnitudes, and Radii of Host Galaxies

Riccardo Scarpa and C. Megan Urry
Space Telescope Science Institute

Renato Falomo
Astronomical Observatory of Padua

Joseph E. Pesce
Eureka Scientific, Inc.

Aldo Treves
University of Insubria

ABSTRACT

We report on a large *HST* imaging survey of BL Lac objects, at spatial resolution $\gtrsim 10$ times better than previous ground-based surveys. We focus on data reduction and analysis, describing the procedures used to model the host galaxy surface brightness radial profiles. A total of 69 host galaxies were resolved out of 110 objects observed, including almost all sources at $z \lesssim 0.5$. We classify them morphologically by fitting with either an exponential disk or a de Vaucouleurs profile; when one fit is preferred over the other, in 58 of 69 cases, it is invariably the elliptical morphology. This is a very strong result given the large number of BL Lac objects, the unprecedented spatial resolution, and the homogeneity of the data set. With the present reclassification of the host galaxy of 1418+546 as an elliptical, there remain no undisputed examples of a disk galaxy hosting a BL Lac nucleus. This implies that, at 99% confidence, fewer than 7% of BL Lacs can be in disk galaxies. The apparent magnitude of the host galaxies varies with distance as expected if the absolute magnitudes are approximately the same, with a spread of ± 1 mag, out to redshift $z \sim 0.5$. At larger redshifts, only 6 of 23 BL Lacs are resolved so the present data do not constrain possible luminosity evolution of the host galaxies. The collective Hubble diagram for BL Lac host galaxies and radio galaxies strongly supports their unification.

Subject headings: BL Lacertae objects — galaxies: structure — galaxies: elliptical

1. Introduction

Determining the properties of AGN host galaxies is an important approach to understanding the AGN phenomenon. The Hubble Space Telescope (*HST*¹), because of its superb spatial resolution, is a valuable tool for this kind of investigation, and indeed this was one of the key science objectives of the *HST*. Not surprisingly, *HST* has been used extensively to image AGN host galaxies (Disney *et al.* 1995; Bahcall *et al.* 1997; Hooper, Impey & Fultz 1997; Falomo *et al.* 1997; Malkan, Gorjian & Raymond 1998; Urry *et al.* 1999; McLeod, Rieke & Storrie-Lombardi 1999; McLure *et al.* 1999).

¹Based on observations made with the NASA/ESA Hubble Space Telescope, obtained at the Space Telescope Science Institute, which is operated by the Association of Universities for Research in Astronomy, Inc., under NASA contract NAS 5-26555.

In the current paradigm for radio-loud AGN, BL Lac objects have relativistically out-flowing jets oriented nearly along the line of sight (Urry & Padovani 1995). Strong relativistic beaming of the jet emission then alters the observed properties of these blazars. Radio-loud AGN pointing at different angles are seen as quasars or radio galaxies — this is the so-called “unification” picture. Proving the correctness of unified schemes is of major importance for our understanding of the true nature of AGN, and is among the most lively topics in modern astrophysics.

Based on preliminary surveys and host galaxy properties, BL Lacs were identified early on with low-luminosity radio galaxies (Schwartz & Ku 1983, Perez-Fournon & Biermann 1984, Ulrich 1989, Browne 1989), i.e., Fanaroff & Riley type I (FR I) radio galaxies (Fanaroff & Riley 1974). Many subsequent studies have supported this hypothesis (Urry & Padovani 1995, and references therein). However, as is often the case in nature, the picture is not so simple and some authors have proposed more complex scenarios in which the parent population includes only some FR Is (e.g., Wurtz, Stocke & Yee 1996), or a mix of FR I and FR II (Kollgaard *et al.* 1996). Indeed, the extended radio morphologies of BL Lacs can be of both FR I and II types (Kollgaard *et al.* 1992), and some of the line emission from FR IIs is weak enough to be BL Lac-like (Laing *et al.* 1994). Thus it may be appropriate to unify BL Lacs more generally with radio galaxies.

The luminosity, size, morphology, and global structure of the BL Lac host galaxy are clearly unaffected by beaming, and so can be a powerful tool to test unified schemes. With ground-based data, several authors have investigated this subject, with consistent results. The BL Lac host galaxies are almost always giant ellipticals, ~ 1 mag brighter than an M^* galaxy, with effective radius of several kiloparsecs (Abraham, McHardy & Crawford 1991; Stickel, Fried & Kühr 1993; Wurtz, Stocke & Yee 1996; Falomo 1996). Similar results have also been found for a handful of BL Lacs observed with *HST* (Falomo *et al.* 1997; Jannuzi, Yanny & Impey 1997; Urry *et al.* 1999). The general properties of the BL Lacs hosts appear consistent with the prediction of the unified models, since the optical counterparts of radio galaxies are always giant ellipticals. However, differences do exist when the average properties of different samples are compared. In particular it is not yet clear whether BL Lac host galaxies are more similar to FR I or to FR II hosts. The issue therefore remains open and is further complicated by claims that some BL Lacs reside in disk galaxies (Halpern *et al.* 1986; Abraham, McHardy & Crawford 1991; Wurtz, Stocke & Yee 1996).

To further investigate this issue, we carried out a large *HST* imaging survey of BL Lac objects, observing 110 objects in “snapshot” mode starting from 132 BL Lacs from seven complete flux-limited samples spanning the redshift range $0.031 < z < 1.34$. Here we describe the data reduction and analysis procedures in some detail, and present the *HST* images, the profile fits, and the associated chi-squared contours. Properties of the host galaxies are discussed in more detail by Urry *et al.* 2000 (hereafter Paper II). This paper is organized as follows. In § 2 we describe observations and data analysis. § 3 reports results, which are more fully described in Paper II, and compares them with previous ground-based surveys. Conclusions are in § 4. Details of individual sources are given in the Appendix, and some of the more peculiar sources, as well as the discovery of an optical jet in PKS 2201+044, have been presented previously by Scarpa *et al.* (1999a,1999b).

2. Observations and Data Analysis

Observations were carried out as *HST* snapshots, which are short exposures obtained during gaps in the observing schedule. A total of 110 targets were selected at random (i.e., depending only on details of

the gaps) from an initial sample of 132 BL Lacs from seven flux-limited samples. These were observed with the Wide Field and Planetary Camera 2 (WFPC2) through the F702W, or in few cases F606W or F555W, filter. For optimal point spread function (PSF) sampling and stability, all objects were placed near the center of the PC chip.

The journal of the observations is reported in Table 1. It includes for each source the original flux-limited sample from which it came, the object type (high- or low-frequency peaked), redshift, and position. Table 1 also lists the date of the *HST* observation, exposure time, filter, and measured surface-brightness of the sky background for that image.

To obtain for each target a final image well exposed both in the inner, bright nucleus and in the outer regions where the host galaxy emission should be well above the wings of the point spread function, we set up a series of exposures with duration ranging from a few tens to up ~ 300 seconds. For each object we usually obtained 3-5 images, which were later combined, to remove cosmic-ray events and improve signal-to-noise ratio. This was done with the CRREJ task available within IRAF, which first masks all saturated pixels, then rescales each image to a common exposure time in order to look for deviant pixels (cosmic rays), and finally adds the images (compensating for pixels eventually masked). The final combined images are shown in Figure 1.

2.1. Flux Calibration

Images were flux calibrated following the prescription of Holtzman *et al.* (1995, their Eq. 9 and Table 10). Namely, we convert F702W and F606W fluxes to Cousin R and Johnson V magnitudes, respectively, with the following transformations:

$$m_R = -2.5 \log(\text{DN}_{\text{F702W}}) + 21.511 + 0.486(V - R) - 0.079(V - R)^2 + 2.5 \log(\text{GN}) + 0.1,$$

$$m_V = -2.5 \log(\text{DN}_{\text{F606W}}) + 22.093 + 0.254(V - I) + 0.012(V - I)^2 + 2.5 \log(\text{GN}) + 0.1,$$

where DN is the digit number per second, GN=2 in the case of gain=7 (our case), and the constant term 0.1 mag corrects for our use of an infinite aperture compared to Holtzman’s 0.5-arcsec aperture. For the sake of clarity, the magnitudes of the few objects observed in filters other than F702W were transformed into the R band; we assumed $V - R = 0.3$ for the point source, and for the host the appropriate $V - R$ color for an elliptical galaxy at the redshift of the BL Lac, as reported in Table 3.

2.2. *HST* Point Spread Function

For studying AGN host galaxies, knowledge of the shape and stability of the PSF is of major importance. We carefully developed a PSF model and tested its reliability extensively. As a first step, to minimize the effects of the spatial variation of the PSF, we placed our targets always at the center of the PC field of view (within 50 pixels). Then we used the theoretical model produced by the Tiny Tim software (Krist 1995), which gives an excellent two-dimensional representation of the PSF within ~ 2 arcsec. Outside this range, particularly in the PC camera, there is a substantial contribution due to large-angle scattered light, which is not included in the Tiny Tim model. Indeed, we found that the radial profiles of several high redshift, unresolved BL Lac objects lay systematically above the Tiny Tim PSF, simply due to scattered light.

To construct the wings of the PSF, we took from the *HST* archive several images of isolated and extremely over-exposed stars. These stars were saturated to such an extent that the PSF wings spread over the three WF chips as well as the PC. Comparing the radial profiles of the different stars, we found that the fraction of scattered light is roughly constant, and only marginally sensitive to telescope focus and position on the chip. We built our final PSF model by smoothly joining, at 2 arcsec, the Tiny Tim inner profile to the average profile of the stars. Figure 2 shows the final composite PSF and individual data points for the unsaturated parts of the stellar images. This composite profile fits very well out to ~ 7 arcsec from the center, spanning a range of more than 15 magnitudes (a factor 10^6 in flux). Small and unpredictable variations of the PSF due to telescope “breathing” were not modeled but were taken into account during the fitting procedure (see § 2.3). For the few sources not at the center of the PC (see notes to the objects), we built a PSF model appropriate to each position.

We give here a simple analytical formula for describing the fraction of scattered light as a function of the total flux I_{PSF} of the Tiny Tim model. On the one dimensional radial profile, the excess light S to be added to the Tiny Tim model at distance r arcsec from the center is:

$$S(r) = A I_{PSF} e^{B r}.$$

The constants A and B depend weakly on wavelength, and are listed in Table 2 for all four filters considered in this paper. The parameter B is quite important as it determines the slope of the scattered light profile, and hence the final slope of the PSF wing.

Properly taking into account the scattered light is of course important in determining whether an object is resolved, but it is also very important when the surface brightness of the host galaxy is comparable to that of the PSF wings. If not included in the PSF model, the scattered light will be attributed to the host, significantly overestimating its luminosity, or leading to spurious galaxy detections. Moreover, a spurious correlation between host and point source luminosity would be introduced, because scattered light and point source luminosity are proportional.

2.3. One-Dimensional Profile and Fitting Procedure

Our snapshot images are typically shorter than would have been ideal for studying extended emission from the host galaxy. As a result, a full two-dimensional analysis of the data has been done by Falomo *et al.* (2000) only for the ~ 30 low redshift sources, for which the host galaxy is well exposed. Instead, we consider here only the azimuthally averaged surface brightness radial profile, thereby increasing the signal-to-noise ratio at the expense of spatial information. In particular, information about asymmetries and/or non-circularities of the host galaxy is lost in the one-dimensional approach.

The median surface brightness reached in our data is $\mu_R = 25.2$ mag/arcsec², 2.5 magnitudes fainter than the sky median surface brightness, allowing us to trace a typical host galaxy out four effective radii. The 1-dimensional radial profiles were determined by averaging the flux over annuli spaced at 1-pixel intervals. Nearby companions and/or stars were masked out and that region of the image simply not considered.

The statistical error associated with the source flux in each annulus was computed considering the statistical noise, readout noise, sky fluctuations, and digitization noise. Sky flux was estimated averaging over several regions uniformly distributed around the chip. The radial surface brightness profiles of all 110 sources is shown in Figure 1.

Radial profiles were fitted with models consisting of PSF plus galaxy; the latter was modeled with either a de Vaucouleurs $r^{1/4}$ law or an exponential law convolved with the PSF. Rather than subtracting the PSF first and analyzing the residuals (the galaxy light), we allowed the PSF normalization and the galaxy brightness to vary simultaneously and independently, minimizing the χ^2 to find the best fit. This avoids the *a priori* determination of the PSF normalization, which can introduce systematic bias in the derived galaxy luminosities.

The fit involves three free parameters varied simultaneously: the PSF total flux, the host galaxy total flux, and the host galaxy effective radius. The best-fit values were then determined from χ^2 minimization. Several details are important to note. First, because the PSF is under-sampled, we excluded the central 0.1 arcsec (the first 3 pixels) from the fit. Second, to account for possible PSF variations introduced by telescope “breathing”, a systematic uncertainty in the PSF model was included. This error was assumed to be 10% of the point source contribution in each pixel, and was added in quadrature to the errors originally associated to the radial profile. In order to actually compute this extra source of error, we need to know at least roughly the PSF normalization. So we first did a coarse fit to normalize the PSF sufficiently well to fix the systematic errors (not to fix the PSF), which are only approximation in any case. We then did the actual fitting for the best-fit PSF and galaxy. The χ^2 distribution was used to evaluate the statistical uncertainties on the three fit parameters.

To determine whether an object was resolved, we fitted the radial profile with a PSF only and with a PSF plus either an exponential disk or a de Vaucouleurs $r^{1/4}$ law; we then compared, via an F-test, the best-fit χ^2 values for the 3 cases. Our threshold was that a galaxy was formally detected when one of the galaxy models was preferred over the PSF only at $> 99\%$ confidence. To be conservative, and to avoid being fooled by large-scale fluctuations in the sky background, we further required that after increasing the sky flux by 1σ , the addition of a galaxy still improved the fit at $> 90\%$ confidence. Similarly, we evaluated which of the two galaxy models was preferred using an F-test at the 99% confidence level.

Fits to the radial profiles are shown in Figure 1 and quantitative results from the one-dimensional fitting are given in Table 3. In addition to the best-fit parameters for de Vaucouleurs and disk models, Table 3 lists a model-independent total apparent magnitude (column 5), integrated to the last point of the radial profiles shown in Figure 1, as well as the chi-squared for a point-source-only fit and the number of data points in the radial profile (column 6). In general, the best-fit PSF normalizations (i.e., nuclear magnitudes) differ for the de Vaucouleurs and disk models, the value associated with the disk model being systematically brighter since it compensates for a relative lack of light in the galaxy center. Only when we can discriminate between the two galaxy models do we have an unambiguous estimate of the point source flux.

We assessed statistical uncertainties in the fit parameters from multi-dimensional χ^2 confidence contours, which are also shown in Figure 1 (for resolved objects). Quoted in Table 3 are the 68% (1σ) confidence uncertainties ($\Delta\chi^2 = 2.3$ for the two parameters of interest, host galaxy magnitude and half-light radius) from the box circumscribing the contour. These represent statistical uncertainties depends only on our estimate of the error bars, and is not related with the fitting procedure. They are in most cases very small, but these smallness should not give the impression that the quantities are actually determined so precisely, because the effect of systematic errors is not included in these values. Indeed, comparing the results obtained from different groups starting from the same set of HST data (e.g., Urry *et al.* 1999), we know that the usual difference in the final estimated host magnitude is larger, some times $\gtrsim 0.2$ mag. In several cases this is much larger than the estimated statistical uncertainty, indicating that systematic errors are dominant.

Finally, for the unresolved BL Lac objects we determined 99% confidence upper limits (statistical errors) to the host galaxy magnitudes ($\Delta\chi^2 = 6.6$ for one parameter of interest, M_{gal}), fixing the effective radius at $r_e = 10$ kpc, slightly larger than the median (to be conservative) for the resolved objects.

2.4. Simulations and Systematic Errors

To test the reliability of our results we performed a series of 140 simulations. We created simulated data by combining a central point source (represented by a two-dimensional composite PSF template) with an elliptical host galaxy ranging in brightness from the point source magnitude to 3 magnitudes fainter. All relevant parameters were adjusted to obtain similar counts per pixel as in the real images, and statistical noise was added. Analysis of the radial profile then followed exactly the same procedure adopted for real objects.

We recover the input parameters with high precision and no systematic biases. The three histograms in Figure 3 show, for each of the three fit parameters (point source magnitude, host galaxy magnitude, and effective radius) the difference between the input parameter value used to generate the simulated data and the fitted parameter derived by minimizing χ^2 . The expected values were recovered to within $\sim 10\%$, with a narrow peak centered at the expected value. The effective radius is the least precisely determined of the three parameters, being off by as much as 0.5 arcsec in our simulations (still much less than disagreement with ground-based measurements; see § 3.2). Most important, no systematic deviations from the expected values are observed, demonstrating that our analysis procedures do not induce spurious trends in the final results. Similar results were obtained when fitting simulated PSF plus disk galaxies, with the effective radius being again the less precisely determined parameter.

3. Results

3.1. Detection Rate of Host Galaxies

Figure 1 shows for each source a gray-scale image representing the central part of the PC camera, together with an isophotal contour which enables a better representation of the nuclear regions. Sources are also described individually in the Appendix. The average radial profile is also shown in Figure 1, with either the best-fit decomposition into PSF plus host galaxy, or the PSF alone for unresolved sources. A total of 72 sources were resolved out to $z \sim 0.6$. In particular, with few exceptions, all 63 sources at $z < 0.5$ were resolved. Both 0851+202 ($z = 0.306$) and 0954+658 ($z = 0.367$) have an extremely bright central point source and it is not surprising that the host remains undetected in our short images. The latter also has uncertain redshift and may actually be more distant. In principle, there may be one more unresolved source at $z < 0.5$, 0735+178, for which only a lower limit to the distance is measured ($z > 0.424$).

For $z > 0.5$ our success rate is much lower, with only 6 of 23 sources resolved. This is not due to a lack of spatial resolution but to the fact that for $z > 0.6$, the F702W filter is mapping the host galaxy spectrum short-ward of the 4000\AA break, so snapshot exposure times are no longer sufficient to detect the rapidly dimming host. Moreover, as the redshift increases, the nuclear component becomes brighter because our sources are selected from flux-limited samples, so contrast with the host increases unless the host galaxies are unusually luminous.

Finally, three resolved objects have no nuclear point source (0145+138, 0446+449 and 0525+713).

Because no nuclear activity was found, their identification as BL Lac objects is dubious (see notes in the Appendix) and we focus on the remaining 69 host galaxies.

To help understand these results, we show in Figure 4 the apparent magnitudes of the nucleus versus the host galaxy (computed assuming elliptical morphology if the host is unclassified). Resolved BL Lac objects fill a 4 mag-wide band inclined at ~ 45 degrees, unresolved objects cluster in the bright-nucleus/faint-galaxy area, and there are no BL Lacs in the bright-galaxy/faint-nucleus zone (where they could easily be resolved). Clearly, the resolved BL Lac objects lie in this central band because of our ability to resolve only those host galaxies with luminosity within few magnitudes of the point source. Fainter galaxies generate the observed upper limits.

Unresolved objects do not follow the same trend. These are all distant sources ($z \gtrsim 0.5$), included in the original flux-limited samples because of their intrinsically bright nuclei (see Figure 2 in Paper II). Indeed, the BL Lacs studied here come either from the optically-selected PG sample or from X-ray- and radio-selected samples with an effective optical flux limit of $m_V \lesssim 20$ mag due to spectroscopic identification. In contrast, the host galaxy had little or no effect on original source selection. Thus the systematically brighter nuclei in the high redshift sources are more likely to out-shine their host galaxies.

The lack of BL Lac objects in the region where the host is most easily detected is easily explained as a consequence of AGN classification. Radio or X-ray sources with a bright nucleus are classified as BL Lac objects, while those with a weak nucleus and prominent host are classified as galaxies. Specifically, for a radio source to be classified as BL Lac, the contrast of the 4000Å break must be smaller than 25% (Dressler & Shectman 1987; Stocke *et al.* 1991; Owen *et al.* 1996). Assuming an intrinsic break of 50% for an elliptical galaxy, and a power-law spectrum for the non-thermal component with spectral index $\alpha = -1.5$ ($F_\nu \propto \nu^\alpha$), close to the steepest values reported for BL Lacs (Falomo, Scarpa & Bersanelli 1994; the limit would be more severe for flatter power laws), sources with $m_{host} < m_{nucleus} + 1.3$ are classified as galaxies. Indeed, radio galaxies fill the lower right-hand corner of the diagram in Figure 4. A few BL Lac objects stray into the galaxy “zone,” likely because of nuclear variability. Although it is obvious, it is worth noting that the average properties of separate AGN classes will be different even when the separation is arbitrary and the properties are continuous across the boundary (e.g., Scarpa & Falomo 1997). In fact, we see a continuous range of absolute nuclear luminosities going from radio galaxies to BL Lac objects (Paper II).

3.2. Comparison With Previous Results

In recent years several authors have published magnitudes of BL Lac host galaxies. The Canada-France-Hawaii (Wurtz, Stocke & Yee 1996), and ESO-NTT (Falomo 1996) imaging surveys of BL Lacs represent the two largest data sets obtained from the ground. There are 24 and 8 objects in common with ours, respectively, so a detailed comparison is possible.

For the host galaxy magnitudes we found good agreement, with modest differences (Figure 5; Wurtz, Stocke & Yee magnitudes were transformed from Gunn r to Cousins R band assuming $r - R = 0.3$ mag). The average magnitude difference is $\langle m_{HST} - m_{ground} \rangle = 0.1$ mag, well within our estimated systematic uncertainty, in spite of all the transformations from the different photometric systems involved. The dispersion is 0.4 mag, showing that the object-to-object discrepancy can be substantial (see the Appendix for one-to-one comparisons).

For the effective radius, the agreement is not as good, probably because this parameter is not as

precisely determined in the fit. This is because r_e depends strongly on the radial profile at large radii, where the signal-to-noise ratio is lowest. The measured values of r_e do not correlate with the intensity of the background, meaning at least statistically our determination of the background is correct. The total magnitude of the host is, however, only marginally affected by a wrong estimate of r_e , because only a minor fraction of the total light is contained in the external regions of the galaxy. For instance, for the BL Lac object 0414+009, observed in both the CFHT and NTT surveys, the estimated effective radii are very different while the total magnitude of the host galaxy is basically the same (and also equal to our value). The average difference between published measures of r_e and ours is 0.2 kpc, only $\sim 2.5\%$ of our median r_e , sufficiently small that we conclude there are no systematic deviations. The dispersion is much larger, 9 kpc, clearly showing the large uncertainty in determining this parameter.

3.3. Host Galaxy Morphology

BL Lac objects are hosted almost universally by elliptical galaxies (Ulrich 1989; Wurtz, Stocke & Yee 1996; Falomo 1996; Kotilainen, Falomo & Scarpa 1998). However, in a small number of cases the host galaxy has been classified as a disk system (Halpern *et al.* 1986; Abraham, McHardy & Crawford 1991; Wurtz, Stocke & Yee 1996). It has been argued that these detections of S0 or spiral host galaxies invalidate the unified model for BL Lacs (see discussion in Urry & Padovani 1995). Thanks to its superior spatial resolution, *HST* is at present the best instrument to distinguish between elliptical and spiral hosts. This is because the radial profiles of the two types of galaxies differ mainly in the center, where ellipticals are substantially more peaked than disks. Ground-based observations usually resolve the host galaxy only at larger radii, where the two galaxy models have similar slopes.

To show how clearly *HST* data can discriminate a de Vaucouleurs from a disk model we show two representative examples in Figure 6. On the left is 0607+711, which was thought to be hosted by a disk galaxy (Wurtz, Stocke & Yee 1996; ground-based study of this source is hampered by a bright star in the field of view). With *HST* we can trace the host galaxy surface brightness profile very close to the nucleus, where the exponential law is completely inadequate to describe the observed profile. Thus we rule out the disk model with high confidence, even though the external part of the radial profile is quite noisy because of the nearby star.

The other example is 1418+546 (OQ 530), which at least three different groups reported was in a disk galaxy (Abraham, McHardy & Crawford 1991; Stickel *et al.* 1993; Wurtz, Stocke & Yee 1996). This time the discrimination between the two models is not easy even at *HST* resolution. The exponential law indeed gives a reasonably good fit, but fails to describe the inner 1.5 arcsec of the observed radial profile (hence it is not surprising that from the ground it was classified as a disk galaxy). In our data, the de Vaucouleurs model is preferred at the 99% confidence level. For a composite disk-plus-bulge model, bulge and disk have similar luminosity. Given the higher mass-to-light ratio of the bulge, the system would still be bulge dominated.

These two cases illustrate the results characteristic of all well-or moderately well-resolved objects. The disk model is always ruled out because it fails to describe the innermost part of the radial profile.

For the sample as a whole, we found unambiguous morphological classifications for 58 hosts, while 14 more hosts could not be classified definitely in one class or the other. For these sources deeper observations are obviously required. All classified hosts but one are ellipticals. The only object that resides in a disk host is 0446+449, which has no nuclear point source and therefore is a galaxy rather than a BL Lac object.

Another BL Lac object that appears to be in a disk galaxy is PKS 1413+135 (Abraham, McHardy & Crawford 1991; Wurtz, Stocke & Yee 1996), which was not in our *HST* sample. Also in this case there is no sign of a nuclear point source, and it has been suggested that the BL Lac lies behind a foreground disk galaxy, or that it is not a BL Lac at all (Stocke *et al.* 1992; Perlman *et al.* 1994; McHardy *et al.* 1994, 1991). Given the lack of nuclear activity in 0446+449 and 1413+135, their identification as BL Lacs is highly questionable.

Three other disk hosts have been reported but none has held up. These include 1415+259 (Halpern *et al.* 1986); 1418+546 (Abraham, McHardy & Crawford 1991; Wurtz, Stocke & Yee 1996), which with 1413+135 implied (at the time) that the fraction of disk galaxies was large; and MS 0205+351 (Wurtz, Stocke & Yee 1996). However, 1415+259 was later reclassified as an elliptical (Romanishin 1992; Wurtz, Stocke & Yee 1996), the host galaxy of 1418+546 has been shown here to be elliptical, PKS 1413+135 is most probably not a BL Lac object, and MS 0205+351 was reclassified as an elliptical (Stocke, Wurtz & Perlman 1995; Falomo *et al.* 1997). Hence, at present there is not a single, unquestionable detection of a disk host galaxy.

In our large *HST* data set, there is not a single BL Lac object hosted by a disk-dominated galaxy. Combining our sample with the CFHT survey, a total of 66 BL Lac hosts have been classified as ellipticals. The probability of randomly extracting a sample of 66 elliptical host galaxies from a mixed distribution is quite low. At 99% confidence, the fraction of disk systems must be $< 7\%$ of the total population. That so few host galaxies can be spirals, and all host galaxies could be ellipticals, strongly reinforces the proposed unification of BL Lac objects and radio galaxies.

3.4. Host Galaxy Apparent Magnitudes and Parent Population

The apparent magnitudes of the BL Lac host galaxies increase with redshift as expected for fixed luminosity, as shown in the Hubble diagram in Figure 7. 90% of the values are within 1 mag of the line corresponding to the median absolute magnitude, $M_R = -23.7$ mag (for $H_0 = 50$ km/s/Mpc and $q_0 = 0$). This holds up to redshift ~ 0.6 , beyond which there are mainly lower limits to the apparent magnitude. This suggests that BL Lac host galaxies are quite similar in luminosity, as they are in morphology. A simple passive evolution model for elliptical galaxies formed at high redshift (Bressan *et al.* 1994) is roughly consistent with the observations; the predicted evolution is in any case very small at $z \lesssim 0.6$. The mean luminosity of the detected host galaxies does increase slightly with redshift, but this is expected at least qualitatively because of several selection effects. More data at $z \gtrsim 0.6$ are necessary to properly address the evolution of the host galaxies.

We now compare the BL Lac host galaxies to three samples of radio galaxies. The first includes FR I and II radio galaxies from a subset of the 2 Jy radio sample (Morganti *et al.* 1993), with redshifts and magnitudes as reported by Wall & Peacock (1985). This sample is interesting because it was selected with a similar radio flux limit as the 1 Jy sample of BL Lacs (Stickel *et al.* 1991), radio morphologies of the sources are well defined, and it covers essentially the same redshift range as the BL Lac objects. The top plot in Figure 8 shows that the BL Lacs host galaxies are essentially indistinguishable from the radio galaxies, across the full redshift range, although at any given redshift the dispersion of radio galaxy magnitudes is larger (because of selection effects explained in § 3.1).

The other two samples of radio galaxies include more objects but at much lower redshift. The Ledlow & Owen (1995) sample includes only sources in clusters, mostly FR Is in the redshift range $0 < z < 0.25$.

The Govoni *et al.* (1999) sample includes FR Is and IIs at somewhat lower redshift $z \lesssim 0.12$, both in clusters and in the field. The bottom plot in Figure 8 shows these radio galaxies in the Hubble diagram. The radio galaxies again have very similar apparent magnitudes to the BL Lac host galaxies, with the same larger dispersion relative to the mean at any given redshift.

This comparison is convincing evidence in favor of the unification of radio galaxies and BL Lacs. For more discussion, see Paper II.

3.5. The BL Lac Nuclei

The Hubble diagram for the BL Lac nuclei, in Figure 9, shows much larger spread than for the host galaxies. The nuclear apparent magnitudes are mostly in the range $15 \lesssim m_R \lesssim 20$, with little dependence on redshift, as expected in flux-limited samples. (The samples plotted here have an effective flux limit of $m_R \sim 20$ mag due to the criterion for optical identification.) The L_{nuc}/L_{host} luminosity ratio should therefore increase with z . For resolved sources, L_{nuc}/L_{host} varies from 0.03 to 5, with a median near 1, reflecting the distinction between BL Lacs and radio galaxies (weak nuclei with bright hosts) and/or our inability to resolve hosts much fainter than the nucleus (see § 3.1).

In § 3.4 we showed that the host galaxies have nearly constant luminosity with redshift (within ± 1 mag). At high redshift, where many BL Lacs are unresolved, we estimate L_{nuc}/L_{host} by varying the (assumed) host galaxy magnitude by ± 1 mag from the sample average. The ranges of expected L_{nuc}/L_{host} are shown in Figure 10 as a function of redshift, along with the measured values for resolved sources. This Figure suggests that L_{nuc}/L_{host} increases significantly with distance, which reflects the bias induced by the flux limit of the BL Lac sample. This means it is misleading to compare this quantity among samples covering different redshift ranges.

4. Conclusions

We reported on a large *HST* survey of BL Lac objects, focusing on the careful procedure for detection and study of the host galaxy. Simulations show that these procedures recover the true source parameters to within the reported errors. We found a simple empirical relation to represent the wings of the *HST* point spread function, at $\gtrsim 2$ arcsec from the center; properly accounting for the scattered light at large radii is essential to not overestimating the galaxy luminosity, and indeed to avoiding false detections.

In the full sample of 110 objects, we detect 72 host galaxies, including essentially all sources at $z \lesssim 0.5$. The data set is large enough and homogeneous enough to allow for a careful assessment of important selection effects. We do not detect bright nuclei with very faint host galaxies, where the PSF swamps the galaxy light, nor do we detect faint nuclei with bright host galaxies, which would have been classified as radio galaxies rather than BL Lac objects.

Three objects, 1ES 0145+138, 1ES 0446+449 and 1ES 0525+713, are very unusual in that they lack a nuclear point source. The morphological types of these three galaxies were determined: 0446+449 is in a disk galaxy, and the other two are in ellipticals. Possibly they are BL Lac objects in a quiescent phase, but a careful re-identification of the optical counterpart is clearly needed.

Of the remaining 69 host galaxies resolved, 58 were classified morphologically, invariably as elliptical.

In the whole sample the only BL Lac residing in a disk galaxy is 0446+449, a possible misidentification. We also reclassify as elliptical the host of 1418+546, previously reported to be a disk. We conclude that in our survey, carried out at a spatial resolution ~ 10 times greater than previously possible from the ground, there are no cases of an unquestionable BL Lac in a disk galaxy. This is particularly significant given the large number of galaxies studied, the homogeneity of the data set, and the careful reduction procedures. At the 99% confidence level, this implies that the fraction of disk galaxies must be smaller than 8% of the total BL Lac populations; adding a few more host galaxies resolved and classified from the ground reduces this fraction to 7%. Our results are thus fully consistent with the hypothesis that BL Lacs reside exclusively in elliptical host galaxies.

Comparison with previous imaging studies of BL Lac objects shows good agreement for the total magnitudes of the host galaxies, as well as good agreement on average for the effective radii, although for individual objects the disagreement can be quite large.

The apparent magnitudes of the host galaxies as a function of distance are consistent with a roughly constant luminosity, with spread of ± 1 mag. There are too few host galaxy detections at $z > 0.6$ to constrain possible luminosity evolution. Finally, comparison of the Hubble diagram for BL Lac hosts and radio galaxies fully supports their unification.

Support for this work was provided by NASA through grant number GO6363.01-95A from the Space Telescope Science Institute, which is operated by AURA, Inc., under NASA contract NAS 5-26555, and by the Italian Ministry for University and Research (MURST) under grant Cofin98-02-32. We thank Jessica Kim for her research on the BL Lac redshifts. RF thanks the *HST* visitor program for hospitality during several visits to STScI. This research made use of the NASA/IPAC Extragalactic Database (NED), operated by the Jet Propulsion Laboratory, Caltech, under contract with NASA, and of NASA’s Astrophysics Data System Abstract Service (ADS).

Results on Individual Objects

0033+595: Two objects, separated by $1''.58$, are found close to the possible optical counterpart of the BL Lac. From the *HST* image alone we could not decide which one is actually the AGN, but based on source color and radio emission the southernmost of the two is the most probable optical counterpart of this BL Lac object (Scarpa *et al.* 1999a). Both objects are unresolved with *HST*.

0118-272: The nuclear source of this distant BL Lac object ($z > 0.559$) is very bright ($M_R = -27.4$ mag). Not surprisingly, the host galaxy is not detected. Some small galaxies are visible in the PC field of view, including one $1''.56$ from the nucleus, at $PA = 71^\circ$.

0122+090: The host galaxy is fully resolved. The radial profile is well described by a de Vaucouleurs law, plus a modest contribution from a nuclear point source. For the host we measure $m_R = 18.9$ mag and $r_e = 1''.05$, similar to the values found by Wurtz, Stocke & Yee (1996), $m_R = 18.35$ mag and $r_e = 1''.6$.

0138-097: The radial profile is largely compatible with the PSF, but a clear excess (> 1 mag) is visible at large radii. This excess of light may be due either to the underlying host galaxy, or to the nearby galaxies that surround the BL Lac. Increasing the sky by 1σ , the radial profile is consistent with the PSF, and we conclude the object remains unresolved. A companion galaxy is visible 1.44 arcsec from the BL Lac and 3

more fainter galaxies are detected within 5 arcsec.

0145+138: As is the case for two other objects from the Einstein Slew survey (0446+449 and 0525+713), no indication of a nuclear point source is found in this BL Lac. The offset of the Slew X-ray source from the proposed optical counterpart is quite large (~ 150 arcsec) and the source was not detected in the Rosat all-sky survey. The absence of nuclear activity, along with the lack of any indication of a power-law continuum in the optical band (see the spectrum in Perlman *et al.* 1996), makes the identification suspicious. The radial profile of the galaxy follows perfectly a de Vaucouleurs law.

0158+003: Clearly resolved with a radial profile very well described by an elliptical host galaxy plus a nuclear point source. A large galaxy is visible $2''.3$ north-west of the BL Lac. It is characterized by a large dust lane, and is most probably an edge-on spiral.

0229+200: This relatively close source is fully resolved in our *HST* image. The host galaxy is elliptical with a radial profile well described by a de Vaucouleurs law. A disk model is ruled out. No companion are visible and the host appears to be absolutely normal.

0235+164: This distant object is unresolved. Our image is not deep enough to enable a full discussion of the very interesting environment that characterizes this BL Lac object (e.g., Falomo 1996). We clearly detect only the southern source located 1.99 arcsec from the BL Lac at position angle 175° . It is unresolved and, given the reported redshift $z = 0.524$, is most probably an AGN.

0257+342: The host galaxy is elliptical with total magnitude $m_R = 17.9$ mag and $r_e = 1''.75$. Our values agree very well with the measurement by Wurtz, Stocke & Yee (1996), $m_R = 17.9$ mag and $r_e = 2''.0$.

0317+178: The object is characterized by a bright nucleus surrounded by a round elliptical host, and a companion galaxy $2''$ south. The host radial profile follows well a de Vaucouleurs law, with best-fit parameters $m_R = 17.6$ mag and $r_e = 3''.25$, moderately larger than found by Wurtz, Stocke & Yee (1996), $m_R = 18.0$ mag and $r_e = 1''.2$. A disk model for the host is ruled out.

0331-365: The source is well resolved into a point source surrounded by a round elliptical host. A disk model is ruled out.

0347-121: The source is clearly resolved with radial profile well described by a point source plus a de Vaucouleurs law. A disk model for the host galaxy is not acceptable. The optical image shows a large interacting system of three galaxies 11.7 arcsec north of the BL Lac. However, there are no indication of connection with the BL Lac.

0350-371: At *HST* resolution the source appears fully resolved, showing a rather elliptical host, which has a radial profile well described by a de Vaucouleurs law. A disk galaxy model for the host is ruled out. A large galaxy is located $6''.2$ west of the BL Lac.

0414+009: At least four independent determinations of the host galaxy magnitude are available for this moderately distant BL Lac object ($z = 0.287$). The two most recent measurements both find $m_R = 17.4$ mag and $r_e \sim 5''$ (Falomo 1996; Wurtz Stocke & Yee 1996). The *HST* image clearly shows the host galaxy surrounding a very bright point source, with a radial profile well described by a point source plus an elliptical galaxy. Our best-fit parameters for the host are $m_R = 17.5$ mag and $r_e = 4''.7$, in good agreement with previous measurements. Despite being the dominant member of a moderately rich cluster (Abell class 0; McHardy *et al.* 1992; Falomo, Pesce & Treves 1993), 0414+009 appears isolated in our image.

0419+194: This distant ($z = 0.512$) source is resolved. The radial profile is better fitted by a de Vaucouleurs law, with best-fit parameters in the usual range for BL Lac hosts and confirming the values reported by Wurtz, Stocke & Yee (1996).

0426-380: This distant object ($z > 1.03$) remains unresolved. A very small companion galaxy is visible $0''.51$ from the BL Lac, at P.A.= 260° .

0446+449: The proposed optical counterpart of this X-ray-selected BL Lac object is a normal disk galaxy with no nuclear point source. This is similar to what is found for two other objects (0145+138 and 0525+713) from the Einstein Slew survey. The coordinates of the proposed optical counterpart (Table 1) differ by $\sim 10''$ from the VLA radio coordinates $\alpha = 04 : 50 : 07.2, \delta = 45 : 03 : 12$ (Perlman *et al.* 1996). Interestingly, none of the several point sources close to the proposed optical counterpart match the VLA coordinates. The original coordinates of the X-ray source are +191,+114 arcsec apart from the VLA position (and therefore also from the optical ones) making the identification highly uncertain.

0454+844: The redshift of this source has recently been determined by Stocke & Rector (1997) to be $z > 1.340$, completely different from the earlier value ($z = 0.112$; reported by Stickel *et al.* 1994 as a private communication by C. Lawrence). Our observation is fully consistent with the object being at high redshift, with no indication of the host galaxy and a radial profile fully consistent with our PSF model.

0502+675: This source turns out to be double: two objects with comparable magnitude and separation of only 0.33 arcsec are clearly visible at *HST* resolution. This is a promising gravitational lens candidate (Scarpa *et al.* 1999a). The brightest source is resolved; however, we were unable to discriminate between different host models.

0506-039: Unfortunately, the BL Lac object falls partly on the PC and partly on the WF camera. We were still able to extract a reliable radial profile, finding the source is fully resolved and the host well described by a de Vaucouleurs law.

0521-365: This well studied nearby object is fully resolved. The radial profile extends up to 14 arcsec from the center and is perfectly described by a de Vaucouleurs law plus a point source. The optical jet is also clearly visible and can be studied as close as 0.3 arcsec from the nucleus (Scarpa *et al.* 1999b).

0525+713: This relatively nearby object ($z = 0.249$) is fully resolved. Unfortunately, due to incorrect coordinates, the object falls on the edge of the WF2 and extends partially on WF3, rather than being in the center of the PC camera. Its radial profile looks like that of a normal elliptical galaxy, well described by a simple de Vaucouleurs law. As is the case for other two objects from the Einstein Slew survey (0145+138 and 0446+449), no indication of nuclear activity was found. The coordinates of the proposed optical counterpart (Table 1), as identified from the published finding chart, differ by $\sim 28''$ from the VLA coordinates (Perlman *et al.* 1996), much more than the stated precision of the VLA radio coordinates ($\sim 1''$). Therefore either there is a mistake in the reported Slew coordinates or in marking the optical counterpart in the finding chart. The absence of a point source at the center of the galaxy together with the lack of any indication of a power-law continuum in the optical band (see the spectrum in Perlman *et al.* 1996), makes the identification suspicious.

0537-441: This distant ($z = 0.896$), bright BL Lac is not resolved. Our 10-minute exposure is largely saturated in the center, allowing the study of the PSF wing up to 7 arcsec from the center. From Figure 1 one can get an idea of the amount of scattered light present in the PC camera (see also the cases of 1553+113, 1424+240). The comparison of this profile with our PSF model shows a perfect match, confirming the object is unresolved and our PSF model correct. Some companion galaxies are visible.

0548-322: This well-studied BL Lac is fully resolved. The host is a large elliptical with radial profile well described by a de Vaucouleurs law. Our measurements for the host galaxy, $m_R = 14.62$ mag and $r_e = 7''.05$, agree exactly with what was found by Wurtz, Stocke & Yee (1996), $m_R = 14.6$ mag and $r_e = 7''.7$, but are quite different from the values reported by Falomo, Pesce & Treves (1995), $m_R = 14.1$ mag and $r_e = 28''$. The reason for such a discrepancy is not clear.

0607+710: This relatively nearby object is clearly resolved. Despite the presence of a bright star that makes the extraction of the radial profile difficult, we can follow it out to 6 arcsec from the center. It is described by a nuclear point source plus an elliptical host galaxy. Contrary to what was found by Wurtz, Stocke & Yee (1996), who reported the host to be a spiral, we are able to rule out a disk model (Fig. 5). Their result may have been influenced by the presence of the bright star.

0622-525: There is no redshift information for this clearly resolved source. The radial profile is well described by an elliptical host galaxy plus a nuclear point source, while a disk model is ruled out.

0647+250: Our 10-minute *HST* exposure of this BL Lac shows a bright point-like object. The image is well exposed and the radial profile can be traced out to 6 arcsec, to a faint surface brightness, $\mu_R \sim 26$ mag arcsec $^{-2}$. The agreement with the PSF model is very good, enabling us to put an interesting lower limit to the host apparent magnitude $m_R > 19.1$ mag. Including 0.35 mag of K correction, and conservatively assuming the host has $M_R = -22.7$ mag, i.e., 1 mag fainter than the median for this sample, our upper limit corresponds to a minimum distance for the source of $z \gtrsim 0.3$.

0706+591: This nearby source ($z = 0.125$) is fully resolved. The radial profile is well described by an elliptical profile plus a nuclear point source, a disk model being definitely ruled out. Within the halo of the BL Lac host galaxy, 4.2 arcsec from the nucleus (projected distance of 12.8 kpc), is a companion disk

galaxy with integrated total magnitude of $m_R = 21$ mag and $r_e = 0''.3$. Some other small galaxies, probably background objects, are present in the PC field of view.

0715-259: The object is resolved into a point source surrounded by a small, rather elongated host galaxy. We were not able to discriminate between disk or de Vaucouleurs models.

0716+714: This BL Lac at unknown distance is a very bright object for which the radial profile can be studied over a large range of surface brightness. The agreement with our PSF model is excellent.

0735+178: For this source only a lower limit to the distance is available ($z > 0.424$; Carswell *et al.* 1974). The apparent magnitude of the nucleus ($V \sim 16.5$ mag) implies it is particularly luminous, which may explain why the host galaxy is not detected. If 0735+178 were at $z = 0.424$, our lower limit for the host galaxy apparent magnitude requires an absolute K-corrected magnitude $M_R > -22.7$ mag.

0737+744: The object located at $z = 0.315$ is resolved. The radial profile is described by a point source plus an elliptical host galaxy. A disk model is ruled out.

0749+540: There is no published redshift for this source, unresolved in our *HST* image. This suggests it may actually be quite distant. To be conservative, assuming the host has $M_R = -22.8$ mag, i.e., 1 mag fainter than the average measured for this sample, and including a K correction of 1 mag, our limit $m_R > 21.9$ mag corresponds to quite a large minimum distance of $z \gtrsim 0.7$.

0754+100: This BL Lac was resolved previously from the ground (Abraham, McHardy & Crawford 1991; Falomo 1996). The estimated absolute magnitude for the host galaxy corresponds to an extremely bright galaxy ($M_R \sim -25$ mag). This result put in question the available redshift ($z = 0.66$) tentatively reported by Persic & Salucci (1986). A galaxy visible 13.6 arcsec north-east of the BL Lac object is known to be at $z = 0.27$ (Pesce, Falomo & Treves 1995). If the host galaxy were at the same redshift, it would have a more reasonable absolute magnitude and would be expected to be resolved from the ground. At *HST* resolution the source appears slightly resolved. The excess over the PSF model can be tentatively described with a de Vaucouleurs model, obtaining an apparent magnitude for the host of $R \sim 19.2$ mag and $r_e \sim 2''$. These figures are in complete agreement with what was found by Falomo (1996) from subarcsecond ground-based imaging ($R \sim 18.9$ mag, $r_e \sim 2''.3$). However, based on our statistical criteria the source remains unresolved and for its host galaxy only an upper limit is reported in Table 3.

0806+524: The redshift for this source has been recently measured by Bade *et al.* (1998), who found the source is moderately nearby ($z = 0.138$). At *HST* resolution 0806+524 is fully resolved and an interesting arc-like structure $1''.93$ south of the nucleus is seen (Scarpa *et al.* 1999a). The radial profile of the host is described by a point source plus an elliptical host. A disk model is ruled out.

0814+425: The reported redshift $z = 0.258$ by Wills & Wills (1976) is based on two weak emission lines identified with MgII(2798Å) and [O II](3727Å). The same authors state that a second spectrogram of apparently similar quality failed to confirm these lines. Later, the spectrum was found featureless on at

least two occasions (Dunlop *et al.* 1989; Stickel *et al.* 1993) so that the proposed redshift has never been confirmed. More recently Lawrence *et al.* (1996) obtained a very high signal-to-noise spectrum, which shows three tiny features at discordant redshift (either 0.245 or 1.25), neither the same as the previously proposed redshift. We therefore assume the redshift is still unknown. Our *HST* image shows a point-like object, with radial profile well described by the adopted PSF model. Conservatively assuming the host has $M_R = -22.8$ mag, i.e., 1 mag fainter than the average measured for this sample, our upper limit on the host galaxy apparent magnitude ($m_R > 20$ mag including 0.9 mag of K correction) corresponds to a minimum distance of $z \gtrsim 0.5$.

0820+225: The profile of this distant object ($z = 0.951$) is stellar. No companions are visible on the frame.

0823+03: The presence of a bright star close to the BL Lac object severely hampers its study. To minimize the impact of the scattered light, we averaged the radial profile only in the 180° opposite the star. The resulting profile lies slightly above the PSF, suggesting the source may be resolved. However, increasing the sky level by 1σ , the source is no longer resolved; hence, we conservatively assume it remains unresolved. This BL Lac was possibly resolved by Wurtz, Stocke & Yee (1996), who estimate an absolute magnitude for the host galaxy of $M_R = -23.9$ mag.

0828+49: The source is resolved, the radial profile being significantly above the PSF. We were not able to discriminate between a disk or elliptical morphology for the host galaxy. The de Vaucouleurs law best fit corresponds to $m_R = 20.26$ mag, the same as reported by Wurtz, Stocke & Yee (1996).

0829+046: This BL Lac object was resolved from the ground by Abraham, McHardy & Crawford (1991) who found $m_R = 16.7$ mag and $r_e = 23''$, and by Falomo (1996), who found $m_R = 17.6$ mag and $r_e = 4''.8$. The source is fully resolved in our *HST* image; however, due to a failure of the telescope tracking, the image is slightly elongated and we were not able to fit properly the central part of the average radial profile (within $1''$ from the center). To describe the profile center properly, we created a PSF model using a star visible in the PC camera. The star was not very bright, permitting us to follow the radial profile only out to ~ 2 arcsec from the center. Because the wings of the PSF profile are only marginally affected by the poor tracking, we smoothly joined the star’s radial profile to the PSF model used for the other objects. Using this customized PSF we were able to describe the observed radial profile quite well. The best-fit de Vaucouleurs law gives $m_R = 16.9$ mag and $r_e = 4''.3$, substantially brighter than reported by Falomo (1996). The two measures of the effective radius, however, agree well. In contrast, Abraham, McHardy & Crawford (1991) report $r_e = 22''$, a value well outside our estimated errors and also much larger than found for any other elliptical galaxy; the fit also seems poor in their Figure 1. We could not discriminate between disk and de Vaucouleurs models.

0851+202: This well-known BL Lac objects was imaged with *HST* by Yanny, Jannuzi & Impey (1997), who reported it was resolved. However, they identify the host with a diffuse structure ~ 0.4 arcsec off-center with respect to the BL Lac nucleus. The same structure was not detected in a much deeper image obtained with the Nordic Optical Telescope (Sillanpää *et al.* 1998), and we suggest it is a ghost image produced within the WFPC2 camera by the bright nucleus. The host was possibly detected by Wurtz, Stocke & Yee (1996), who report $m_R = 19.8$ mag. The average radial profile derived from our *HST* image, which was a

short exposure of only 5 minutes, shows a perfect match with the PSF model. This is the nearest source ($z = 0.306$) that remains unresolved.

0922+74: This moderately distant source ($z = 0.638$) is resolved. The host is an intrinsically very bright elliptical ($M_R = -24.6$ mag including K correction of 1.34 mag). A disk model is ruled out. From the ground, the host galaxy has never been clearly detected. Wurtz, Stocke & Yee (1996) report a marginal detection with $m_R \sim 21.9$ mag, more than a magnitude fainter than our measurement $m_R \sim 20.25$ mag.

0927+500: The BL Lac object is fully resolved into a point source surrounded by a round elliptical host. A disk model is ruled out. Several small galaxies are visible in the frame, suggesting the source may be member of a small cluster.

0954+685: This source is among the nearest ($z = 0.367$) in our sample that remain unresolved. The lower limit to the host galaxy apparent magnitude is $m_R \sim 19.6$ mag, a value that coincides with that found by Wurtz, Stocke & Yee (1996), who claimed it was marginally resolved. The fact that this moderately nearby source was unresolved with *HST* is most probably due to the brightness of the nucleus ($m_R \sim 16.1$ mag) during our observation. We note, however, that the redshift deserves some comment. There are two determinations, both quite uncertain. Lawrence *et al.* (1986) report the marginal detection of very faint [OIII]5007Å emission and Mg b band absorption lines at $z = 0.368$. However, they concluded that the redshift is a “tentative value, requiring confirmation.” Later, Stickel, Fried & Kühr (1993) detected [OII] 3727Å and CaII 3933,3968Å at the same redshift ($z = 0.367$), but no one line has been detected twice. It would therefore be highly desirable to have a firmer determination of the distance to this object.

0958+21: The BL Lac object is resolved and surrounded by several galaxies. Among them is a big nice spiral. The nuclear point source was very faint during the observation, allowing a detailed study of the host galaxy. The radial profile is consistent with a simple de Vaucouleurs law, while a disk model is ruled out.

1011+496: The redshift of this object is uncertain, being based on the possible membership of the BL Lac in the cluster Abell 950, and some galaxies are indeed detected in the field of view, at $z = 0.20$ (Wisniewski *et al.* 1986). In our *HST* image the source is clearly resolved, with an average radial profile well described by a point source plus an elliptical host galaxy. A disk model for the host is not acceptable.

1028+511: A reliable redshift of $z = 0.361$ based on CaII H&K absorption lines has been recently reported by Polonski *et al.* (1997), a value somewhat larger than the previously reported $z = 0.239$. The object is resolved, and its radial profile is well described by a de Vaucouleurs law plus a nuclear point source.

1044+54: The BL Lac object is resolved and the radial profile is well described by a nuclear point source plus a de Vaucouleurs law. There is no reported redshift for this object. Conservatively assuming the host has $M_R = -24.8$ mag, i.e., 1 mag brighter than the average measured for this sample, and including a K correction of 1.4 mag, the measured apparent magnitude $m_R = 20.05$ mag implies $z < 0.65$.

1104+384: The source is fully resolved with *HST*. The host galaxy is elliptical with quite normal

isophotes, indicating no tidal stress due to the large companion galaxy $14''.2$ to the north-east. The nuclear point source is perfectly centered on the host galaxy. A disk model is ruled out.

1106+24: The BL Lac object is resolved with radial profile well described by a point source plus a de Vaucouleurs law; however, a disk model for the host cannot be ruled out. The redshift of the object is unknown. We set a tentative upper limit for the distance assuming, to be conservative, the host has luminosity $M_R = -24.8$ mag, i.e., 1 mag brighter than the average measured for this sample, and including a K correction of 1.4 mag, the measured apparent magnitude $m_R = 19.6$ mag implies $z < 0.6$.

1133+168: In our *HST* image the BL Lac object is very close to the PC edge, preventing a complete study of its radial profile. Despite this problem and the moderately large redshift ($z = 0.460$, Fichtel *et al.* 1994), the source appears fully resolved and well described by a point source plus an elliptical host galaxy. A disk model is ruled out. Several other galaxies are visible on the WF camera.

1136+704: This well-studied nearby source is fully resolved. The radial profile is perfectly described by a de Vaucouleurs law plus a nuclear point source. The magnitude of the point source is ill defined as our profile is largely saturated on the center.

1144-379: This distant source ($z = 1.048$) is unresolved.

1147+245: The BL Lac object is unresolved, its radial profile being fully consistent with the PSF model. No redshift information is available. To be conservative, assuming the host galaxy has $M_R = -22.8$ mag, i.e., 1 mag fainter than the average measured for this sample, and including a K correction of 0.9 mag, our limit $m_R > 20.7$ mag for the host apparent magnitude corresponds to a tentative minimum distance of $z > 0.45$.

1207+394: At *HST* resolution this moderately distant source is resolved. The host is elliptical with best-fit parameters $m_R = 20.30$ mag and $r_e = 1''.2$, corresponding to a very bright host $M_R = -24.4$ mag. A disk model is ruled out.

1212+078: This nearby source ($z = 0.136$) is fully resolved. The host is a large, round elliptical. A disk model is definitely ruled out.

1215+303: The host galaxy is a large, round elliptical. A disk model is ruled out. Two galaxies are detected superimposed on the host galaxy, at projected distance of $1''.43$ and $2''.76$, together with several other small galaxies located all around the BL Lac object.

1218+30: The BL Lac object is well resolved and the host galaxy is an elliptical. The clear detection of the host galaxy is consistent with the source being at the recently determined redshift $z = 0.182$ (Bade *et al.* 1998). No companion galaxies were detected.

1221+245: This source was observed in the I band with *HST* by Jannuzi, Yanni & Impey (1997) with exposure time longer than the F606W (V band) snapshot observation presented here. The source is resolved in both cases and the derived parameters for the host galaxy agree well with the I-band values (see Urry et al. 1999). The color $V - I = 1.8$ mag. is fully consistent with the expectation (1.6 mag) for a normal elliptical galaxy at $z = 0.218$.

1229+643: This nearby BL Lac object ($z = 0.164$) is fully resolved. The elliptical host looks quite symmetric despite the presence of a companion galaxy located $3''.36$ to the south-west. A disk model for the host is ruled out. Our best-fit de Vaucouleurs model corresponds to $m_R = 16.4$ mag and $r_e = 2''.0$, which agrees well with what was found by Wurtz, Stocke & Yee (1996), $m_R = 16.5$ mag and $r_e = 2''.9$

1239+069: This BL Lac from the Einstein Slew survey remains unresolved. We note that in our *HST* survey we resolve all sources at $z \lesssim 0.3$, and the detected host galaxies show only a small dispersion in luminosity. It is therefore surprising that this source, reported at $z = 0.150$ (Perlman *et al.* 1996), remains unresolved. At that distance, our upper limit for the host luminosity of $m_R > 22.3$ mag would correspond to an absolute magnitude $M_R = -17.6$ mag, extremely weak for a BL Lac host galaxy. Because the available redshift is based on the detection of very weak lines, it may be erroneous. In absence of a more reliable determination of the distance, we have assumed it is unknown.

1246+586: This BL Lac at unknown distance is unresolved. Conservatively assuming the host has $M_R = -22.8$ mag, i.e., 1 mag fainter than the average measured for this sample, our lower limit on the host apparent magnitude ($m_R > 20.2$ mag including 1 mag of K correction) corresponds to a tentative minimum distance of $z \gtrsim 0.5$.

1248-293: The source is clearly resolved. The host is elliptical, a disk galaxy being ruled out. Some other galaxies are detected in the PC camera.

1249+174: This distant BL Lac ($z = 0.644$) is not resolved.

1255+244: This nearby source is fully resolved in our *HST* image. The host galaxy is a large, circular elliptical. A disk model is ruled out.

1320+084: This source at unknown distance remains unresolved. The lower limit to the apparent magnitude of the host galaxy is $m_R > 22.7$ mag. Assuming the host has an absolute magnitude $M_R = -22.8$ mag, i.e., 1 mag fainter than the average measured for this sample, yields a tentative minimum distance of $z \gtrsim 0.5$.

1402+042: This moderately distant source ($z = 0.340$) remains unresolved. The radial profile is largely consistent with the PSF model and the two profiles become fully consistent after increasing the sky by 1σ . It is however interesting that our lower limit to the host galaxy apparent magnitude, $m_R > 19.4$ mag, is very similar to the limit from Wurtz, Stocke & Yee (1996), and is well within the range of luminosities observed for BL Lac hosts. Unlike the plots for other unresolved sources, Figure 1 shows the radial profile

of the upper limit galaxy.

1407+595: This source was observed through the F606W filter in order to obtain useful color information when combined with the F814W observation obtained by Jannuzi, Yanni & Impey (1997). The best-fit de Vaucouleurs model gives $m_V = 20.48$ mag and $r_e = 1''.75$, while from the F814W observation Urry *et al.* (1999) derived $m_I = 18.38$ mag and $r_e = 1''.4$. The agreement for r_e is good, and the derived color $V - I = 2.1$ is consistent with the expected value ($V - I = 2.6$) for an early-type galaxy at $z = 0.495$.

1418+54: The source is fully resolved. The bright nuclear source (saturated in our image) is surrounded by a large elliptical galaxy. A smaller but sizeable galaxy, possibly an edge-on spiral, is visible 10.7 arcsec away. Several other galaxies are visible in the WF field of view. Our best-fit de Vaucouleurs model for the host gives $m_R = 16.1$ mag and $r_e = 3''.6$, one half magnitude brighter and 50% larger than reported by Wurtz, Stocke & Yee (1996), $m_R = 16.6$ mag and $r_e = 2''.4$

1422+58: This distant source ($z = 0.638$, Bade *et al.* 1998) remains unresolved at *HST* resolution.

1424+24: This bright BL Lac source remains unresolved in our *HST* data. The image is well exposed, enabling us to trace the radial profile out to 7 arcsec from the nucleus, a range of ~ 15 magnitudes in surface brightness. As in other similar cases, the profile of the PSF model agrees perfectly with the BL Lac profile over this very large range in brightness. Conservatively assuming the host has $M_R = -22.8$ mag, i.e., 1 mag fainter than the average measured for this sample, our lower limit on the host apparent magnitude ($m_R > 21.0$ mag including 0.9 mag of K correction) corresponds to a minimum distance of $z \gtrsim 0.5$.

1426+42: The object is resolved into a bright nuclear source surrounded by an elliptical galaxy, with average radial profile perfectly described by a point source plus a de Vaucouleurs model out to 7 arcsec from the center. A disk model is ruled out.

1437+39: This fully resolved object is surrounded by several galaxies, suggesting it is the main member of a small cluster. The radial profile is well described by a point source plus a de Vaucouleurs law. A disk model is ruled out.

1440+122: This BL Lac object is a member of a dumbbell system. At the position of the BL Lac nucleus (the eastern object in Figure 1), two point sources are detected, separated by only $0''.29$. The fainter is at position angle 70° . This is an interesting gravitational lens candidate (Scarpa *et al.* 1999a). The BL Lac host is an elliptical galaxy. A disk model is ruled out.

1458+228: Despite the moderately large distance ($z = 0.235$) and the short exposure time of our observation (320 s), we detected the host galaxy of this BL Lac. The radial profile is consistent with either de Vaucouleurs or disk models.

1514-241: AP Lib is a nearby BL Lac object for which a number of studies have been carried out (e.g.,

Abraham, McHardy & Crawford 1991). The *HST* image shows a bright point source surrounded by a large, round elliptical host.

1517+656: This source has a recently reported redshift of $z > 0.7$ (Beckmann *et al.*, private communication) based on the presence of MgI and FeII absorption lines. At *HST* resolution 1517+656 shows a rather unusual and very interesting morphology, with three arcs surrounding the nuclear point source, possibly tracing an Einstein ring (Scarpa *et al.* 1999a). The average radial profile of the central object is largely consistent with our PSF model, indicating little contribution from a possible host galaxy.

1519-273: This source at unknown redshift remains unresolved. We set a tentative lower limit to the distance assuming the host has absolute magnitude $M_R = -22.8$ (i.e., 1 mag fainter than the average measured for this sample), which gives $z \gtrsim 0.4$.

1533+53: The source is saturated and its radial profile shows at the largest radii some deviations from the PSF model. After increasing the sky level by 1σ , the two profiles became consistent, so we conservatively consider the source unresolved. This result is consistent with the BL Lac object being at $z = 0.89$ as tentatively reported by Bade *et al.* (1998).

1534+014: The BL Lac is resolved. The host is a large, round elliptical. A disk galaxy is ruled out. The best-fit de Vaucouleurs model gives $m_R = 18.2$ mag and $r_e = 2''.0$, corresponding to a galaxy significantly smaller than that reported by Wurtz, Stocke & Yee (1996), $m_R = 17.4$ mag and $r_e = 4''.3$.

1538+149: For this distant BL Lac object ($z = 0.605$) we have both a snapshot image in the F606W filter and pointed observations in F814W (Urry *et al.* 1999). In the shorter snapshot image, the object is only barely resolved, but the host galaxy parameters are consistent with those found in the deeper pointed observation.

1544+820: This relatively bright BL Lac at unknown redshift is not resolved. Using our lower limit for the host apparent magnitude, and conservatively assuming its intrinsic luminosity is $M_R = -22.8$ mag (i.e., 1 mag fainter than the average measured for this sample) we find a tentative lower limit for the distance of $z \gtrsim 0.35$.

1553+113: This well known, bright BL Lac object is heavily saturated in our image. Thanks to the brightness of the source, we trace its radial profile down to a surface brightness 16 magnitudes fainter than the central peak. Nonetheless, the source remains unresolved.

1704+604: The object is resolved. The nuclear point source was quite faint during our observation, allowing the study of the galaxy radial profile in to the very center. The radial profile is well described by a de Vaucouleurs law, a disk model being ruled out.

1722+119: This bright BL Lac at unknown redshift remain unresolved. We use our lower limit

$m_R > 21.4$ mag for the host apparent magnitude to set a tentative lower limit to the distance of $z \gtrsim 0.55$, assuming a host absolute magnitude of $M_R = -22.8$ mag, i.e., 1 mag fainter than the average measured for this sample. This is much larger than either the initially proposed redshift of $z = 0.018$ (Griffiths 1989), not confirmed by Veron-Cetty & Veron (1993), or $z = 0.159$ reported by Wurtz, Stocke & Yee (1996) (without any further reference). Our result suggests both values may be incorrect and we assume the redshift of 1722+119 remains unknown.

1728+502: This nearby ($z = 0.055$) BL Lac object is fully resolved. The host is a large, round elliptical. A disk model is ruled out.

1738+47: This source remains unresolved, with the azimuthally averaged radial profile fully consistent with the PSF model. We use our limit for the host apparent magnitude, $m_R > 20.5$ mag, to set a lower limit to the distance of $z > 0.45$, assuming a host galaxy absolute magnitude of $M_R = -22.8$ mag, i.e., 1 mag fainter than the average measured for this sample. This is larger than the value reported in literature ($z = 0.316$). We carefully checked the source of this redshift and were not able to assess its reliability. Indeed, NED reports $z = 0.316$ and refers to Xu *et al.* (1995), who in turn refer to Xu *et al.* (1994), who reported the source spectrum as featureless! Therefore we conclude the redshift is unknown.

1745+504: This source is clearly resolved and several other galaxies are present in the PC camera. The nuclear point source was very faint during the observation. A disk model for the host is ruled out.

1749+701: This bright, distant source remain unresolved.

1749+096: This moderately distant BL Lac object is resolved into a point source surrounded by a galaxy that remains morphologically unclassified. The best-fit de Vaucouleurs model gives $m_R = 18.8$ mag and $r_e = 3''.0$, quite different from what was found by Wurtz, Stocke & Yee (1996), $m_R = 17.7$ mag and $r_e = 7''.1$. This may be due to the several stars that surround this low galactic latitude BL Lac object, which make it difficult to study from the ground.

1757+70: In our *HST* image the object is unfortunately located close to one edge of the WF4 chip. The radial profile can be extracted only for 180 degree and due to the presence of three stars has to be truncated ~ 3 arcsec from the center. In spite of this limiting factor, and the relatively high redshift ($z = 0.407$), the source is resolved and the host classified as elliptical. The host has apparent magnitude $m_R = 19.6$ mag, consistent with the value $m_R = 19.5$ mag in Wurtz, Stocke & Yee (1996).

1803+784: This moderately distant object remain unresolved.

1807+698: In our *HST* image 3C 371 is characterized by the presence of a jet first discovered by Nilsson *et al.* (1997) from the ground. The *HST* image was discussed by Scarpa *et al.* (1999b). The elliptical host galaxy is easily visible.

1823+568: For this distant source ($z = 0.664$) we have a snapshot *HST* image in the F606W filter and a

pointed *HST* observation in the F814W filter (Urry *et al.* 1999). In both cases the host galaxy is detected, making 1823+568 the most distant resolved BL Lac object in our sample.

1853+671: This nearby source is clearly resolved. The host galaxy is definitely elliptical, a disk model being ruled out.

1914-194: The source is clearly resolved. The average radial profile is consistent with either de Vaucouleurs and disk models. Few companion galaxies are detected in the PC field of view.

1959+650: This nearby source is fully resolved. The radial profile is very well described by a point source plus a de Vaucouleurs model. A disk galaxy is definitely ruled out.

2005-489: This well studied nearby source is fully resolved. The host galaxy is a large, round elliptical, with an extremely bright nucleus which dramatically impedes its observation from the ground. The radial profile is well described by a point source plus a de Vaucouleurs model with $m_R = 14.5$ mag and $r_e = 5''.6$, consistent with the values found by Falomo (1996), $m_R = 14.8$ mag and $r_e = 6''$. A disk galaxy is ruled out.

2007+777: In our *HST* data the source is clearly resolved. However, the short exposure time prevents us from discriminating between an elliptical or a disk host.

2037+521: The source, fully resolved, is characterized by an elliptical host galaxy. A small companion galaxy is visible 0.6 arcsec away from the nucleus (PA= 135°), projecting well inside the host.

2131-021: This distant source ($z = 1.285$) is not resolved. No companions detected.

2143+070: The radial profile of this moderately close BL Lac is well described by a point source plus a de Vaucouleurs law. A disk galaxy is ruled out. The best-fit parameters for the host are $m_V = 18.76$ mag and $r_e = 2''.1$. These values agree with what was found in a deeper F814W observation by Jannuzi, Yanni & Impey (1997), confirmed by Urry *et al.* (1999), $m_I = 17.15$ mag and $r_e = 1''.8$. The color is $V - I = 1.61$, as expected for an elliptical galaxy at $z = 0.237$.

2149+173: This object, for which there is no redshift information, remains unresolved in our *HST* data. Conservatively assuming the host has $M_R = -22.8$ mag (i.e., 1 mag fainter than the average measured for this sample), and including 0.7 magnitudes of K correction, a tentative lower limit for the distance of $z \gtrsim 0.4$ can be set.

2200+420: The *HST* observation of the eponymous BL Lac object shows the source is fully resolved, albeit dominated by a very bright nucleus. The galaxy is elliptical, as already found by Wurtz, Stocke & Yee (1996), with apparent magnitude $m_R = 15.5$ and $r_e = 4''.8$. These values are ~ 1 mag fainter and a factor of 2 smaller than found by Wurtz Stocke & Yee (they found $r_e = 10''.2$). In spite of the low redshift, these large differences are probably due to the very bright nucleus.

2201+044: This nearby source is fully resolved. The host is an elliptical galaxy and our best-fit values for the apparent magnitude and effective radius are fully consistent with those reported by Wurtz, Stocke & Yee (1996). The most interesting result for this BL Lac is the detection of the optical counterpart of the radio jet (see Scarpa *et al.* 1999b).

2240-260: This BL Lac object is unresolved. This result is consistent with the source being at $z = 0.774$ (Stickel *et al.* 1993), based on the detection of two very weak emission lines that have never been confirmed.

2254+074: We have both pointed (F814W) and snapshot (F606W) observations of this BL Lac object. The source is fully resolved and classified as elliptical in both cases. The best-fit parameters are $m_V = 17.4$ mag and $r_e = 4''.9$ for the F606W observation, and $m_I = 15.9$ mag and $r_e = 4''.8$ for the F814W observation. The derived color is $V - I = 1.5$, as expected for an early-type galaxy at $z = 0.190$.

2326+174: This BL Lac object has a round elliptical host galaxy. A disk model for the host is ruled out.

2344+514: A large elliptical host galaxy dominates the *HST* image of this nearby BL Lac object. Its radial profile follows particularly well a de Vaucouleurs law.

2356-309: This nearby source is fully resolved. The host is an elliptical, with a radial profile well fitted by a de Vaucouleurs law. A disk model is ruled out. Our values for the host galaxy magnitude and effective radius, $m_R = 17.21$ mag and $r_e = 1''.85$, agree well with the values reported by Falomo *et al.* (1991), $m_R = 17.24$ mag and $r_e = 3''.5$.

REFERENCES

- Abraham R.G., McHardy I.M. & Crawford C.S. 1991, MNRAS 252, 482
Bade N., Beckmann V., Douglas N.G., *et al.* 1998, A&A 334, 459
Bahcall J.N., Kirhakos S., Saxe D.H. & Schneider 1997, ApJ 479, 642
Bressan A., Chiosi C. & Fagotto F. 1994, ApJS 94, 63
Browne I.W.A. 1989, in BL Lac Objects, ed. L. Maraschi, T. Maccaro, & M. H. Ulrich, p 401
Carswell R.F., Strittmatter P.A., Williams R.E., Kinman T.D. & Serkowski K. 1974, ApJ 190, L101
Chiaberge M., Capetti A. & Celotti A. 1999, A&A, in press
Disney M.J., Boyce P.J., Blades J.C. *et al.* 1995 Nature 376, 150
Dressler A. & Shectman S.A. 1987, AJ 94, 899
Dunlop J.S., Peacock J.A., Savage A., Lilly S.J., Heasley J.N., Simon A.J.B. 1989, MNRAS 238, 1171
Fanaroff B. & Riley J.M. 1974, MNRAS 167, 31P
Falomo R. 1991, AJ 101, 821

- Falomo R. 1996, MNRAS 283, 241
- Falomo R., Kotilainen J., Pursimo T., Sillanpää A., Takalo L. & Heidt J. 1997, A&A 321, 374
- Falomo R., Pesce J.E., & Treves A. 1993 ApJ 411, L63
- Falomo R., Pesce J.E., & Treves A. 1995 ApJ 438, L9
- Falomo R., Scarpa R., & Bersanelli M. 1994, ApJS 93, 125
- Falomo R., Urry C.M., Pesce J.E., Scarpa R., Giavalisco M. & Treves A. 1997, ApJ 476, 113
- Falomo R., Urry C.M., Pesce J.E., Scarpa R., & Treves A. 2000 in preparation
- Fichtel C.E., Bertsch D.L., Chiang J. *et al.* 1994 ApJS 94, 551
- Fukugita M, Shimasaku K. & Ichikawa T. 1995, PASP 107, 945
- Govoni F., Falomo R., Fasano G. & Scarpa R. 1999, A&A in press
- Green R.F., Schmidt M. & Liebert J. 1986, ApJS 61, 305
- Griffiths R.E., Wilson A.S., Ward M.J., Tapia S. & Ulvestad J.S. 1989, MNRAS 240, 33
- Halpern J.P., Impey C.D., Bothun G.D., Tapia S., Skillman E.D. Wilson A.S. & Meurs E.J.A. 1986 ApJ 302, 71
- Holtzman, J. A., Burrows, C. J., Casertano, S., Hester, J. J., Trauger, J. T., Watson, A. M., & Worthey, G. 1995, PASP, 107, 1065
- Hooper E.J., Impey C.D., & Foltz C.B. 1997, ApJ, 480, L95
- Jannuzi B.T., Yanny B. & Impey C. 1997, ApJ 491, 146
- Kollgaard R.I., Palma C., Laurent-Muehleisen S.A. & Feigelson E.D. 1996, ApJ 465, 115
- Kollgaard R. I., Wardle J. F. C., Roberts D. H., & Gabuzda D. C. 1992, AJ 104, 1687
- Kotilainen J.K., Falomo R. & Scarpa R. 1998, A&A 336, 479
- Krist, J. 1995, in *Astronomical Data Analysis, Software and Systems IV*, eds. R. Shaw et al., (San Francisco: Astr. Soc. Pac.), p. 349
- Laing R.A. 1994, in *The Physics of Active Galaxies*. ASP Conference Series, G.V. Bicknell, M.A. Dopita, and P.J. Quinn, Eds., Vol. 54, p. 227
- Lamer G., Brunner H. & Staubert R. 1996, A&A 311, 384
- Lawrence C.R., Pearson T.J., Readhead A.C.S. & Unwin S.C. 1986 AJ 91, 494
- Lawrence C.R., Zucker J.R., Readhead A.C.S., Unwin S. C., Pearson T.J., & Xu W. 1996 ApJS 107, 541
- Ledlow M.J. & Owen F.N. 1995, AJ 109, 853
- Malkan M.A., Gorjian V. & Tam R. 1998, ApJS 117, 25
- McHardy I.M., Abraham R.J., Crawford C.S., Ulrich M.-H., Mock P.C. & Vanderspek R.K. 1991, MNRAS, 249, 742
- McHardy I.M., Luppino G.A., George I.M., Abraham R.J., Cooke B.A. 1992, MNRAS 256, 655
- McHardy I.M., Merrifield M.R., Abraham R.J., & Crawford C.S. 1994, MNRAS 268, 681
- McLeod K.K., Rieke J.H. & Storrie-Lombardi L.J. 1999, ApJ 511, L67
- McLure R.J., Kukula M.J., Dunlop J.S., Baum S.A., O’Dea C.P. & Hughes D.H. 1999, MNRAS in press
- Morganti R., Killen N.E.B. & Tadhunter C.N. 1993, MNRAS 263, 1023

- Morris S.L., Stocke J.T., Gioia I.M., Schild R.E., Wolter A., Maccacaro T. & Della Ceca R. 1991, ApJ 380, 49
- Nilsson K., Heidt J., Pursimo T., Sillanpää A., Takalo L.O. & Jäger 1997 ApJ 484, L107
- Owen F.N., Ledlow M.J. & Keel W.C. 1996, AJ 111, 53
- Perez-Fournon I & Biermann P. 1984, A&A 130, L13
- Perlman E.S., Stocke J.T., Wang Q.D. & Morris S.L. 1996, ApJ 456, 451
- Perlman E.S., Stocke J.T., Shaffer D.B., Carilli C.L. & MA C. 1994 ApJ 424, 69
- Persic M. & Salucci P. 1986, in *Structure and Evolution of Active Galactic Nuclei*, ed. G. Giuricin, F. Mardirossian, M. Mezzetti and M. Ramella, p. 657
- Pesce J.E., Falomo R. & Treves A. 1995, AJ 110, 1554
- Piccinotti G., Mushotzky R.F., Boldt E.A., Holt S.S., Marshall F.E., Serlemitsos P.J. & Shafer R.A. 1982 ApJ 253, 485
- Polomski E., Vennes S., Thorstensen J.R., Mathioudakis M. & Falco E.E. 1997 ApJ 486, 179
- Remillard R. *et al.* 1999, in preparation
- Romanishin W. 1992, ApJ 401, L65
- Sambruna R., Maraschi L. & Urry C.M. 1996, ApJ 463, 444
- Scarpa R. & Falomo R. 1997, A&A 325, 109
- Scarpa R., Urry C.M., Falomo R., Pesce J.E., Webster R., O'Dowd M. & Treves A. 1999a, ApJ 521, in press
- Scarpa R., Urry C.M., Falomo R. & Treves A. 1999b, ApJ 526, in press
- Schachter J.F., Stocke J.T., Perlman E., *et al.* 1993, ApJ 412, 541
- Schwartz, D. A., Brissenden, R. J. V., Tuohy, R.T. R., Feigelson, E. D., Hertz, P. L., & Remillard, R. A., 1989, in *BL Lac Objects*, ed. L. Maraschi, T. Maccacaro, M.-H. Ulrich (Berlin: Springer-Verlag), p. 208
- Schwartz D.A. & Ku W.H.M. 1983, ApJ 266, 459
- Sillanpää A., Takalo L.O., Nilsson K., Pursimo T. & Pietilä 1998, in *BL Lac Phenomenon*, A.S.P. Conf. Ser., Vol. 159, ed. L.T. Takalo and A. Sillanpää, p. 395
- Stickel M., Fried J.W., & Kühr H. 1993, A&AS 98, 393
- Stickel M. & Kühr H. 1994 A&AS, 103, 349
- Stickel M., Meisenheimer K. & Kühr H. 1994, A&AS 105, 211
- Stickel M., Padovani P., Urry C.M., Fried J.W., & Kuhr H. 1991, ApJ 374, 431
- Stocke J.T., Morris S.L., Gioia I.M., Maccacaro T., Schild R., Wolter A., Fleming T.A. & Henry J.P. 1991, ApJS 76, 813
- Stoke J.T. & Rector T.A. 1997, ApJ 489, L17
- Stocke J.T., Wurtz R., Wang Q., Elston R. & Jannuzi B.T. 1992 ApJ 400, L17
- Stocke J.T., Wurtz R.E. & Perlman E.S. 1995, ApJ 454, 55
- Ulrich, M.H. 1989, in *BL Lac Objects*, ed. L. Maraschi, T. Maccacaro, & M. H. Ulrich, p 45
- Urry C. M. & Padovani P. 1995, PASP 107, 803

- Urry C. M., Falomo R., Scarpa R., Pesce J. E., Treves A. & Giavalisco M. 1999, ApJ 512, 88
- Urry C. M., Scarpa R., O’Dowd M., Falomo R., Giavalisco M. Pesce J. E., Treves A. & 2000, ApJ submitted (Paper II)
- Véron-Cetty M. P. & Véron P. 1993, A&AS 100, 521
- Wall J.V. & Peacock J.A. 1985, MNRAS 216, 173
- Wills D. & Wills B.J. 1976, ApJS 31, 143
- Wisniewski W.Z., Sitko M.L. & Sitko A.K. 1986 MNRAS 219, 299
- Wurtz R., Stoke J.T. & Yee H.K.C. 1996, ApJS 103, 109
- Yanny B., Jannuzi B.T. & Impey C. 1997, ApJ 484, L113
- Xu W., Lawrence C.R., Readhead A.C.S. & Pearson T.J. 1994, AJ 108, 395
- Xu W., Readhead A.C.S., Pearson T.J., Polatidis A.G. & Wilkinson P.N. 1995, ApJS 99, 297

Table 2. Scattered Light Coefficients

Filter	A	B
F814W	5.6×10^{-4}	-0.42
F702W	7.3×10^{-4}	-0.50
F606W	1.3×10^{-3}	-0.48
F555W	8.0×10^{-4}	-0.48

Table 1. Journal of the Observations

Object	Cat., name ^(a)	Type ^(b)	z ^(c)	RA ^(d) (J2000)	Dec. (J2000)	Date	Exp. (sec)	Filter	$\mu_R(sky)$ ^(e)
0033 + 595	SLEW	H	...	00:35:52.74	59:50:04.3	3/03/96	1060	F702W	21.57 ± 0.06
0118 - 272	1Jy	L	> 0.559	01:20:31.56	-27:01:23.8	30/06/99	440	F702W	22.54 ± 0.10
0122 + 090	EMSS	H	0.339	01:24:44.51	09:18:49.3	11/10/97	500	F702W	21.78 ± 0.07
0138 - 097	1Jy	L	0.733	01:41:25.76	-09:28:43.4	28/09/96	840	F702W	22.21 ± 0.10
0145 + 138	SLEW	H	0.124	01:48:29.68	14:02:18.2	19/01/99	500	F702W	21.62 ± 0.10
0158 + 001	EMSS	H	0.229	02:01:06.14	00:34:00.8	19/10/96	500	F702W	22.08 ± 0.01
0229 + 200	HEAO-A3	H	0.139	02:32:48.60	20:17:16.9	22/12/96	305	F702W	21.76 ± 0.22
0235 + 164	1Jy	L	0.940	02:38:38.94	16:37:00.2	7/12/98	200	F702W	21.59 ± 0.09
0257 + 342	EMSS	H	0.247	03:01:03.73	34:41:01.6	14/10/97	500	F702W	22.13 ± 0.09
0317 + 183	EMSS	H	0.190	03:19:51.83	18:45:34.8	6/10/97	500	F702W	21.96 ± 0.03
0331 - 362	EMSS	H	0.308	03:33:12.18	-36:19:47.4	29/10/96	500	F702W	22.47 ± 0.26
0347 - 121	HEAO-A3	H	0.188	03:49:23.14	-11:59:27.1	26/03/97	500	F702W	21.68 ± 0.10
0350 - 371	EMSS	H	0.165	03:51:54.50	-37:03:44.5	3/05/97	500	F702W	22.00 ± 0.08
0414 + 009	HEAO-A3	H	0.287	04:16:52.48	01:05:24.2	3/04/97	500	F702W	21.34 ± 0.05
0419 + 194	EMSS	H	0.512	04:22:18.38	19:50:54.1	9/03/96	840	F702W	21.20 ± 0.04
0426 - 380	1Jy	L	> 1.030	04:28:40.38	-37:56:20.2	28/03/96	1060	F702W	22.41 ± 0.01
0446 + 449	SLEW	H	0.203	04:50:06.64	45:03:04.8	26/02/96	300	F702W	21.13 ± 0.10
0454 + 844	1Jy	L	> 1.340	05:08:42.93	84:32:04.7	14/03/96	320	F702W	22.99 ± 0.05
0502 + 675	HEAO-A3	H	0.314	05:07:56.25	67:37:24.4	2/03/96	740	F702W	22.06 ± 0.05
0506 - 039	HEAO-A3	H	0.304	05:09:38.12	-04:00:45.1	10/12/98	500	F702W	20.64 ± 0.05
0521 - 365	HEAO-A3	L	0.055	05:22:57.89	-36:27:31.0	6/05/96	305	F702W	21.73 ± 0.01
0525 + 713	SLEW	H	0.249	05:31:37.51	71:21:50.8	26/04/96	500	F702W	21.84 ± 0.03
0537 - 441	1Jy	L	0.896	05:38:50.33	-44:05:08.7	29/03/96	614	F702W	22.74 ± 0.15
0548 - 322	HEAO-A2	H	0.069	05:50:40.55	-32:16:15.9	12/01/99	320	F702W	21.98 ± 0.23
0607 + 710	EMSS	H	0.267	06:13:43.33	71:07:26.7	23/04/96	500	F702W	22.04 ± 0.14
0622 - 525	EMSS	H	...	06:23:37.88	-52:57:57.1	28/03/96	1060	F702W	21.81 ± 0.08
0647 + 250	HEAO-A3	H	...	06:50:46.52	25:03:00.3	7/09/96	590	F702W	21.05 ± 0.04
0706 + 591	HEAO-A3	H	0.125	07:10:30.05	59:08:19.6	26/04/96	500	F702W	22.09 ± 0.04
0715 - 259	SLEW	H	...	07:18:04.77	-26:08:11.6	30/03/97	1260	F702W	22.23 ± 0.06
0716 + 714	1Jy	H	...	07:21:53.42	71:20:36.2	3/06/96	614	F702W	21.90 ± 0.06
0735 + 178	1Jy	L	> 0.424	07:38:07.36	17:42:18.3	18/05/97	440	F702W	20.85 ± 0.03
0737 + 744	EMSS	H	0.315	07:44:05.26	74:33:57.6	26/02/96	320	F702W	22.70 ± 0.07
0749 + 540	4C+54.15	L	...	07:53:01.34	53:52:59.5	16/03/97	500	F702W	22.33 ± 0.11
0754 + 100	L	* 0.67	07:57:06.66	09:56:34.8	2/04/97	605	F702W	22.09 ± 0.11	
0806 + 524	SLEW	H	0.138	08:09:49.15	52:18:58.7	11/09/96	610	F702W	22.00 ± 0.01
0814 + 425	1Jy	L	...	08:18:15.95	42:22:45.4	8/04/97	500	F606W	21.88 ± 0.06
0820 + 225	1Jy	L	0.951	08:23:24.82	22:23:03.2	3/04/96	1060	F702W	21.80 ± 0.06
0823 + 033	1Jy	L	0.506	08:25:50.34	03:09:24.5	12/04/97	840	F702W	22.06 ± 0.11
0828 + 493	1Jy	L	0.548	08:32:23.20	49:13:20.0	27/02/96	840	F702W	22.24 ± 0.06
0829 + 046	HEAO-A3	L	0.180	08:31:48.69	04:29:36.2	17/03/96	200	F702W	22.25 ± 0.02
0851 + 202	1Jy, OJ287	L	0.306	08:54:48.88	20:06:30.0	12/04/97	305	F606W	22.02 ± 0.13
0922 + 749	EMSS	H	0.638	09:28:02.78	74:47:18.8	7/12/98	840	F702W	22.27 ± 0.10
0927 + 500	SLEW	H	0.188	09:30:37.62	49:50:24.9	24/03/96	320	F702W	22.73 ± 0.96
0954 + 658	1Jy	L	* 0.367	09:58:47.14	65:33:54.9	17/03/97	440	F702W	21.65 ± 0.07
0958 + 210	EMSS	H	0.344	10:01:42.38	20:48:17.7	9/04/96	840	F702W	22.07 ± 0.08
1011 + 496	HEAO-A3	H	0.200	10:15:04.14	49:26:00.3	21/05/96	320	F702W	22.21 ± 0.02
1028 + 511	HEAO-A3	H	0.361	10:31:18.46	50:53:36.4	20/05/96	320	F702W	22.29 ± 0.02
1044 + 549	SLEW	H	...	10:47:45.90	54:37:41.0	27/02/96	1060	F702W	22.30 ± 0.08
1104 + 384	HEAO-A3, MRK421	H	0.031	11:04:27.24	38:12:31.2	5/05/97	302	F702W	21.49 ± 0.18
1106 + 244	SLEW	H	...	11:09:16.14	24:11:19.6	16/04/96	1260	F702W	22.07 ± 0.00
1133 + 161	EMSS	H	0.460	11:36:17.49	16:01:53.1	7/03/96	1060	F702W	22.08 ± 0.01
1136 + 704	HEAO-A3, MRK180	H	0.045	11:36:26.27	70:09:27.3	12/04/96	610	F702W	21.66 ± 0.09
1144 - 379	1Jy	L	1.048	11:47:01.47	-38:12:11.2	27/04/96	740	F702W	22.59 ± 0.09
1147 + 245	1Jy	H	...	11:50:19.25	24:17:54.4	22/03/97	720	F702W	22.38 ± 0.08
1207 + 396	EMSS	H	0.615	12:10:26.52	39:29:08.5	5/02/99	840	F702W	22.50 ± 0.13
1212 + 078	SLEW	H	0.136	12:15:10.95	07:32:04.5	30/03/97	740	F702W	21.99 ± 0.06
1215 + 303	SLEW	H	0.130	12:17:52.10	30:07:00.1	03/04/99	614	F702W	23.00 ± 0.03
1218 + 304	HEAO-A2	H	0.182	12:21:21.91	30:10:36.6	26/05/96	320	F702W	22.43 ± 0.06
1221 + 245	EMSS	H	0.218	12:24:24.16	24:36:23.2	7/02/99	500	F606W	22.07 ± 0.15
1229 + 643	EMSS	H	0.164	12:31:31.60	64:14:17.9	7/04/96	320	F702W	22.81 ± 0.24
1239 + 069	SLEW	H	...	12:41:48.22	06:36:00.7	12/03/97	500	F702W	22.08 ± 0.09
1246 + 586	PG	H	...	12:48:18.69	58:20:29.0	4/04/96	840	F702W	22.50 ± 0.04

Table 1—Continued

Object	Cat., name ^(a)	Type ^(b)	z ^(c)	RA ^(d) (J2000)	Dec. (J2000)	Date	Exp. (sec)	Filter	μ_R (<i>sky</i>) ^(e)
1248 – 296	SLEW	H	0.370	12:51:34.89	–29:58:42.9	8/03/96	840	F702W	22.49 ± 0.01
1249 + 174	SLEW	H	0.644	12:51:45.34	17:11:17.9	24/03/97	840	F702W	22.28 ± 0.06
1255 + 244	SLEW	H	0.141	12:57:31.94	24:12:39.9	14/04/97	610	F702W	22.27 ± 0.08
1320 + 084	SLEW	H	...	13:22:54.93	08:10:10.5	07/02/99	1260	F702W	22.07 ± 0.06
1402 + 042	EMSS	H	* 0.340	14:04:50.90	04:02:02.3	10/12/98	320	F702W	21.03 ± 0.10
1407 + 595	EMSS	H	0.495	14:09:23.49	59:39:40.6	23/05/97	840	F606W	22.81 ± 0.12
1418 + 546	PG, OQ 530	L	0.152	14:19:46.53	54:23:14.4	24/10/96	614	F702W	22.40 ± 0.11
1422 + 580	HEAO-A3	H	0.683	14:22:38.79	58:01:54.9	8/04/96	500	F702W	21.33 ± 0.08
1424 + 240	PG	H	...	14:27:00.38	23:48:00.7	27/04/96	740	F702W	22.48 ± 0.11
1426 + 428	HEAO-A3	H	0.129	14:28:32.66	42:40:20.6	30/05/96	320	F702W	22.81 ± 0.25
1437 + 398	PG	L	...	14:39:17.44	39:32:42.6	17/04/96	840	F702W	22.59 ± 0.08
1440 + 122	SLEW	H	0.162	14:42:48.35	12:00:40.5	7/05/97	320	F702W	22.36 ± 0.14
1458 + 224	EMSS	H	0.235	15:01:01.82	22:38:06.3	10/05/97	320	F702W	22.57 ± 0.33
1514 – 241	1Jy, AP Librae	H	0.049	15:17:41.89	–24:22:19.4	5/05/97	320	F702W	21.91 ± 0.11
1517 + 656	HEAO-A3	H	> 0.7	15:17:47.60	65:25:23.9	1/02/97	614	F702W	22.51 ± 0.17
1519 – 273	1Jy	L	...	15:22:37.68	–27:30:10.3	25/03/97	1260	F702W	22.05 ± 0.05
1533 + 535	SLEW	H	* 0.89	15:35:00.72	53:20:37.4	26/03/96	1260	F702W	22.89 ± 0.12
1534 + 014	EMSS	H	0.312	15:36:46.72	01:37:59.8	11/05/97	500	F702W	22.18 ± 0.09
1538 + 149	1Jy	L	0.605	15:40:49.48	14:47:46.2	21/05/96	440	F606W	22.61 ± 0.06
1544 + 820	SLEW	H	...	15:40:15.56	81:55:07.3	3/03/96	740	F702W	22.35 ± 0.13
1553 + 113	PG	H	...	15:55:43.05	11:11:23.6	8/09/96	610	F702W	22.02 ± 0.11
1704 + 604	EMSS	H	0.280	17:05:34.82	60:42:15.8	13/03/97	460	F702W	22.36 ± 0.12
1722 + 119	HEAO-A3	H	...	17:25:04.36	11:52:15.2	10/03/97	740	F702W	21.96 ± 0.08
1728 + 502	HEAO-A3, IZw187	H	0.055	17:28:18.61	50:13:10.9	21/05/96	320	F702W	22.59 ± 0.22
1738 + 476	S4	L	...	17:39:57.06	47:37:58.6	30/04/97	500	F702W	22.48 ± 0.12
1745 + 504	SLEW	H	...	17:46:32.37	50:28:10.7	27/02/96	1060	F702W	22.53 ± 0.01
1749 + 096	1Jy	L	0.320	17:51:32.80	09:39:01.1	12/05/97	320	F702W	22.58 ± 0.21
1749 + 701	1Jy	L	0.770	17:48:32.86	70:05:51.5	24/03/97	580	F702W	22.48 ± 0.11
1757 + 703	EMSS	H	0.407	17:57:12.98	70:33:38.7	7/04/96	840	F702W	22.63 ± 0.03
1803 + 784	1Jy	L	0.684	18:00:45.68	78:28:04.2	7/04/97	440	F702W	22.55 ± 0.14
1807 + 698	1Jy, 3c 371	L	0.051	18:06:50.59	69:49:28.1	1/06/97	302	F555W	21.56 ± 0.23
1823 + 568	1Jy	L	0.664	18:24:07.13	56:51:01.8	30/12/96	840	F606W	22.31 ± 0.07
1853 + 671	SLEW	H	0.212	18:35:52.00	67:13:55.0	31/03/96	320	F702W	22.98 ± 0.03
1914 – 194	HEAO-A3	H	...	19:17:44.85	–19:21:31.1	28/02/96	840	F702W	20.48 ± 0.01
1959 + 650	HEAO-A3	H	0.048	19:59:59.87	65:08:54.1	9/01/97	302	F702W	22.60 ± 0.32
2005 – 489	1Jy	H	0.071	20:09:25.36	–48:49:54.0	30/05/96	610	F702W	22.13 ± 0.13
2007 + 777	1Jy	L	0.342	20:05:30.95	77:52:43.8	10/05/97	440	F702W	22.19 ± 0.10
2037 + 521	SLEW	H	...	20:39:23.64	52:19:50.6	25/01/97	1060	F702W	21.83 ± 0.04
2131 – 021	1Jy	L	1.285	21:34:10.31	–01:53:16.4	4/04/96	840	F702W	20.92 ± 0.02
2143 + 070	EMSS	H	0.237	21:45:52.34	07:19:28.0	13/05/97	500	F606W	21.91 ± 0.07
2149 + 173	PKS	L	...	21:52:24.81	17:34:38.1	14/08/96	840	F702W	22.39 ± 0.07
2200 + 420	1Jy	L	0.069	22:02:43.34	42:16:40.5	7/12/98	302	F702W	22.15 ± 0.28
2201 + 044	HEAO-A3	L	0.027	22:04:17.69	04:40:02.3	13/12/98	610	F702W	21.42 ± 0.07
2240 – 260	1Jy	L	* 0.774	22:43:26.38	–25:44:30.9	18/05/97	840	F702W	21.79 ± 0.05
2254 + 074	1Jy	L	0.190	22:57:17.29	07:43:12.9	13/05/97	320	F606W	21.52 ± 0.06
2326 + 174	SLEW	H	0.213	23:29:03.32	17:43:30.3	30/01/97	300	F702W	21.22 ± 0.06
2344 + 514	SLEW	H	0.044	23:47:04.82	51:42:17.4	18/01/97	614	F702W	22.01 ± 0.09
2356 – 309	HEAO-A3	H	0.165	23:59:07.84	–30:37:40.5	8/05/97	320	F702W	21.92 ± 0.10

^(a)Sources were selected from seven flux limited samples. References are as follow. 1 Jy: Stickel et al. 1991; S4: Stickel & Kühr 1994; PG: Green et al. 1986; HEAO-A2: Piccinotti et al. 1982; HEAO-A3: Remillard et al. 1999, Schwartz et al. 1989 ; EMSS: Morris et al. 1991; Slew: Schachter et al. 1993, Perlman et al. 1996.

^(b)Spectral energy distribution type is H for High frequency peaked or L for low frequency peaked BL Lac objects, depending on whether $\log F_{1 \text{ keV}}/F_{5 \text{ GHz}}$ is greater than or less than 5.5, respectively. Classification mostly derived from Lamer *et al.* 1996, Sambruna *et al.* 1996, and Perlman *et al.* 1996.

^(c)Reported redshift for the BL Lac object. Most HBL redshifts were determined from weak stellar absorption features arising in the BL Lac host galaxy; LBL redshifts were more often derived from (weak) emission lines, in some cases a single line. Particularly uncertain values are indicated with asterisks (*); for details, see the Appendix.

^(d)Coordinates of the light centroid of the source as measured on the HST image, using the *HST* astrometric solution. Errors are ± 0.01 seconds of time and ± 0.05 arcsecs.

^(e) Sky surface brightness in (*mag/arcsec*²) with associated 1σ error.

Table 3. Parameters of Model Fits to Azimuthally Averaged Surface Brightness Profiles ^(a)

Object	(V-R) (b)	z (c)	Host (d)	m _R (e)	χ _ν ² /pnt (f)	de Vaucouleurs law fit				Disk galaxy fit			
						m _R point (g)	m _R host (h)	r _e (i)	χ _ν ² (f)	m _R point (g)	m _R host (h)	r _e (i)	χ _ν ²
0033 + 595	1.10	...	N	18.06	2.1/32	18.23 ± 0.08	> 20.00	17.75 ± 0.08	> 21.0
0118 - 272	1.50	> 0.559	N	15.87	1.2/64	15.78 ± 0.10	> 19.09	15.78 ± 0.10	19.43
0122 + 090	1.10	0.339	E	18.75	388/68	21.98 ± 0.25	18.88 ± 0.04	1.05 ± 0.10	0.82	21.28 ± 0.0	19.38 ± 0.0	1.3 ± 0.0	71
0138 - 097	1.48	0.733	N	17.48	9.8/68	17.68 ± 0.05	> 20.19	17.38 ± 0.05	> 20.6
0145 + 138	0.70	0.124	E	17.02	171/117	...	16.96 ± 0.03	1.75 ± 0.05	0.10
0158 + 001	0.85	0.229	E	17.73	27/121	18.38 ± 0.06	18.27 ± 0.03	1.90 ± 0.10	3.20	18.38 ± 0.0	18.95 ± 0.0	2.05 ± 0.0	21.0
0229 + 200	0.71	0.139	E	15.82	17.4/222	18.58 ± 0.35	15.85 ± 0.01	3.25 ± 0.07	5.75	16.8 ± 0.0	16.45 ± 0.0	2.33 ± 0.0	37.3
0235 + 164	1.35	0.940	N	17.66	0.55/20	18.18 ± 0.10	> 19.75	18.0 ± 0.1	> 20.25
0257 + 342	0.89	0.247	E	17.71	400/96	19.18 ± 0.30	17.93 ± 0.01	1.75 ± 0.12	0.93	18.78 ± 0.0	18.71 ± 0.0	1.7 ± 0.0	64
0317 + 183	0.78	0.190	E	17.31	2000/95	18.28 ± 0.05	17.59 ± 0.01	3.25 ± 0.10	5.5	18.28	18.0	3.5	340
0331 - 362	1.03	0.308	E	17.65	13/141	19.03 ± 0.10	17.81 ± 0.02	3.10 ± 0.20	1.35	17.55 ± 0.06	18.51 ± 0.02	3.05 ± 0.12	23.8
0347 - 121	0.78	0.188	E	17.24	7.6/129	18.28 ± 0.15	17.72 ± 0.01	1.25 ± 0.05	2.12	16.84 ± 0.0	18.7 ± 0.01	2.10 ± 0.05	12.3
0350 - 371	0.74	0.165	E	16.68	1850/113	18.03 ± 0.15	17.08 ± 0.01	1.70 ± 0.07	1.38	18.28 ± 0.0	17.76 ± 0.0	2.50 ± 0.0	908
0414 + 009	0.98	0.287	E	16.15	10/181	16.08 ± 0.05	17.49 ± 0.02	4.70 ± 0.50	1.23	16.1 ± 0.05	18.24 ± 0.03	3.80 ± 0.10	1.50
0419 + 194	1.45	0.512	E	19.27	2.2/33	19.53 ± 0.17	21.05 ± 0.15	0.40 ± 0.07	2.98	19.18 ± 0.09	22 ± 0.40	0.70 ± 0.30	7.2
0426 - 380	1.28	> 1.030	N	17.77	0.8/67	18.08 ± 0.05	> 21.13	17.94 ± 0.05	> 21.9
0446 + 449	0.80	0.203	D	16.19	26/141	16.18 ± 0.05	3.35 ± 0.1	1.13
0454 + 844	1.07	> 1.340	N	17.91	1.5/33	18.20 ± 0.04	> 22.37	18.2 ± 0.04	> 23.0
0502 + 675	1.10	0.314	U	17.17	3.6/51	17.33 ± 0.10	18.90 ± 0.09	0.60 ± 0.07	1.29	17.23 ± 0.08	20.10 ± 0.13	1.05 ± 0.07	0.86
0506 - 039	1.02	0.304	E	17.79	21/27	18.83 ± 0.08	18.37 ± 0.02	0.70 ± 0.05	4.47	18.38 ± 0.07	18.94 ± 0.03	0.55 ± 0.05	12.8
0521 - 365	0.64	0.055	E	14.12	200/278	15.28 ± 0.10	14.60 ± 0.01	2.80 ± 0.07	1.41	14.72 ± 0.0	15.42 ± 0.0	4.5 ± 0.02	96
0525 + 713	0.89	0.249	E	17.54	100/60	...	17.49 ± 0.01	1.98 ± 0.01	15.5
0537 - 441	1.37	0.896	N	15.28	0.9/118	15.83 ± 0.04	> 19.66	15.68 ± 0.0	> 21.1
0548 - 322	0.65	0.069	E	14.92	350/193	16.93 ± 0.10	14.62 ± 0.01	7.05 ± 0.15	0.88	16.48 ± 0.0	15.62 ± 0.0	2.5 ± 0.0	99.2
0607 + 710	0.93	0.267	E	17.39	11/120	18.23 ± 0.10	17.83 ± 0.02	2.40 ± 0.12	1.36	18.08 ± 0.0	18.43 ± 0.0	2.50 ± 0.0	19.1
0622 - 525	1.10	...	E	18.50	8.9/69	18.83 ± 0.18	19.37 ± 0.04	1.50 ± 0.20	1.74	18.08 ± 0.02	20.15 ± 0.05	1.55 ± 0.08	15.3
0647 + 250	1.10	...	N	15.73	1.2/117	15.18 ± 0.03	> 19.10	15.18 ± 0.02	> 19.5
0706 + 591	0.70	0.125	E	16.10	90/81	17.53 ± 0.07	15.94 ± 0.01	3.05 ± 0.07	2.45	16.68 ± 0.0	16.64 ± 0.0	1.7 ± 0.0	34.0
0715 - 259	1.10	...	U	17.99	2.2/63	18.13 ± 0.03	20.02 ± 0.04	0.45 ± 0.05	1.62	17.75 ± 0.08	21.15 ± 0.15	0.80 ± 0.05	1.20
0716 + 714	1.10	...	N	15.19	2.4/190	14.18 ± 0.01	> 20.00	14.28 ± 0.01	> 18.7
0735 + 178	1.30	> 0.424	N	16.39	1.5/67	16.58 ± 0.07	> 20.44	16.58 ± 0.03	> 20.8
0737 + 744	1.04	0.315	E	17.14	5.9/70	17.88 ± 0.15	18.01 ± 0.08	2.10 ± 0.45	0.29	17.35 ± 0.10	18.71 ± 0.09	1.70 ± 0.15	0.68
0749 + 540	0.8	...	N	16.15	1.5/79	16.23 ± 0.03	> 21.90	16.28 ± 0.01	> 22.0
0754 + 100	1.51	* 0.67	N	15.88	2.9/129	16.03 ± 0.00	> 18.69	15.78 ± 0.03	> 19.4
0806 + 524	1.08	0.138	U	15.71	23/146	15.98 ± 0.02	16.62 ± 0.01	1.45 ± 0.03	6.77	15.48 ± 0.04	17.30 ± 0.01	2.0 ± 0.02	6.24
0814 + 425	0.91	...	N	18.16	1.9/31	18.99 ± 0.07	> 20.90	18.99 ± 0.05	> 21.6	1.80 ± 1.80	...
0820 + 225	1.36	0.951	N	19.63	1.9/26	19.98 ± 0.02	> 21.91	19.88 ± 0.03	> 22.5
0823 + 033	1.44	0.506	N	17.40	2.7/53	17.78 ± 0.11	> 20.18	17.63 ± 0.10	> 20.9
0828 + 493	1.49	0.548	U	18.59	3.9/47	18.93 ± 0.12	20.26 ± 0.10	0.65 ± 0.1	1.27	18.78 ± 0.08	21.29 ± 0.10	0.90 ± 0.05	1.01
0829 + 046	0.76	0.180	U	15.59	7.0/159	15.88 ± 0.07	16.94 ± 0.04	4.30 ± 0.75	1.71	15.65 ± 0.03	17.72 ± 0.02	3.30 ± 0.15	2.35
0851 + 202	1.02	0.306	N	15.22	0.98/95	14.99 ± 0.06	> 18.53	15.14 ± 0.02	> 19.3
0922 + 745	1.52	0.638	E	19.46	7.07/27	20.13 ± 0.07	20.25 ± 0.05	0.85 ± 0.10	1.55	19.73 ± 0.05	20.80 ± 0.03	0.70 ± 0.03	6.37
0927 + 500	0.78	0.188	E	17.05	6.6/84	17.48 ± 0.30	17.62 ± 0.05	2.0 ± 0.45	0.45	17.2 ± 0.10	18.32 ± 0.07	1.75 ± 0.17	1.14
0954 + 658	1.17	* 0.367	N	15.96	1.3/85	16.08 ± 0.06	> 19.60	16.08 ± 0.05	> 20.0
0958 + 210	1.11	0.344	E	18.72	6.6/89	21.48 ± 0.40	18.93 ± 0.01	0.82 ± 0.04	1.48	20.28 ± 0.0	19.58 ± 0.0	1.0 ± 0.0	99
1011 + 496	0.8	0.200	U	15.86	6.3/114	15.88 ± 0.05	17.30 ± 0.02	1.80 ± 0.12	2.09	15.53 ± 0.08	18.13 ± 0.05	2.00 ± 0.05	3.10
1028 + 511	1.16	0.361	U	16.51	4.9/94	16.48 ± 0.10	18.55 ± 0.08	1.80 ± 0.35	2.19	16.58 ± 0.05	19.4 ± 0.07	2.20 ± 0.15	1.93
1044 + 549	1.10	...	E	19.26	8.1/52	19.88 ± 0.15	20.05 ± 0.05	0.95 ± 0.10	2.44	19.28 ± 0.0	20.7 ± 0.0	1.1 ± 0.0	12.7
1104 + 384	0.62	0.031	E	12.94	210/263	13.78 ± 0.08	13.29 ± 0.02	3.95 ± 0.05	4.25	12.78 ± 0.0	13.96 ± 0.0	5.0 ± 0.0	13.6

Table 3—Continued

Object	(V-R) (b)	z (c)	Host (d)	m _R (e)	χ^2_V/pnt (f)	de Vaucouleurs law fit				Disk galaxy fit			
						m _R point (g)	m _R host (h)	r _e (i)	χ^2_ν (f)	m _R point (g)	m _R host (h)	r _e (i)	χ^2_ν
1106 + 244	1.10	...	U	17.89	6.2/93	18.28 ± 0.08	19.57 ± 0.04	1.80 ± 0.20	2.05	17.95 ± 0.05	20.35 ± 0.06	1.85 ± 0.10	2.02
1133 + 161	1.38	0.460	E	18.42	9.5/66	20.28 ± 0.18	19.83 ± 0.04	1.55 ± 0.23	1.58	19.4 ± 0.10	20.58 ± 0.05	1.35 ± 0.07	23.6
1136 + 704	0.63	0.045	E	14.41	2000/251	16.15 ± 0.04	14.45 ± 0.00	3.10 ± 0.02	1.60	14.58 ± 0.0	15.17 ± 0.0	4.4 ± 0.0	102
1144 − 379	1.27	1.048	N	17.16	5.6/52	17.28 ± 0.00	> 23.03	17.28 ± 0.0	> 23.3
1147 + 245	1.10	...	N	16.67	1.2/87	16.87 ± 0.04	> 20.70	16.88 ± 0.04	> 20.9
1207 + 349	1.52	0.615	E	19.00	62.2/39	19.48 ± 0.05	20.30 ± 0.05	1.20 ± 0.15	2.55	18.18 ± 0.0	20.95 ± 0.03	1.0 ± 0.0	8.18
1212 + 078	0.71	0.136	E	15.72	400/247	16.38 ± 0.10	16.02 ± 0.01	3.40 ± 0.10	3.16	15.28 ± 0.0	16.75 ± 0.0	4.45 ± 0.02	6.04
1215 + 303	0.87	0.130	E	15.10	555/143	14.55 ± 0.01	16.05 ± 0.01	8.35 ± 0.20	2.99	14.18 ± 0.0	16.70 ± 0.0	6.30 ± 0.03	14.4
1218 + 304	0.77	0.182	E	15.76	9.5/152	15.68 ± 0.10	17.12 ± 0.03	2.60 ± 0.30	1.85	15.53 ± 0.05	17.87 ± 0.04	3.0 ± 0.15	3.72
1221 + 245	0.83	0.218	E	16.53	19.6/60	16.89 ± 0.05	18.63 ± 0.06	1.25 ± 0.25	1.13	16.69 ± 0.02	19.48 ± 0.07	1.40 ± 0.05	1.82
1229 + 643	0.74	0.164	E	16.23	300/141	18.03 ± 0.30	16.38 ± 0.01	2.00 ± 0.07	1.78	16.48 ± 0.0	17.06 ± 0.0	2.3 ± 0.0	6.40
1239 + 069	1.10	...	N	18.35	2.9/38	18.45 ± 0.05	> 22.30	18.48 ± 0.06	> 22.4
1246 + 586	1.10	...	N	16.32	1.1/118	15.66 ± 0.01	> 21.20	15.67 ± 0.03	> 21.6
1248 − 296	1.18	0.370	E	18.09	75/112	18.83 ± 0.08	18.87 ± 0.02	1.10 ± 0.05	2.16	18.01 ± 0.0	19.77 ± 0.0	1.0 ± 0.0	13.0
1249 + 174	1.51	0.644	N	18.43	1.4/36	18.51 ± 0.07	> 21.90	18.58 ± 0.04	> 22.2
1255 + 244	0.71	0.141	E	16.44	350/201	17.08 ± 0.05	16.72 ± 0.01	2.50 ± 0.05	3.53	16.08 ± 0.0	17.45 ± 0.0	3.3 ± 0.0	20.8
1320 + 084	0.61	...	N	18.87	2.64/22	18.93 ± 0.10	> 22.3	15.93 ± 0.0	> 22.6
1402 + 041	1.11	* 0.340	N	16.39	2.29/45	16.38 ± 0.01	> 19.38	16.49 ± 0.03	> 15.6
1407 + 595	1.43	0.495	E	18.47	20/58	18.84 ± 0.05	19.04 ± 0.05	1.75 ± 0.38	2.13	18.46 ± 0.05	19.73 ± 0.05	1.60 ± 0.10	4.03
1418 + 546	0.73	0.152	E	15.56	360/151	15.68 ± 0.06	16.10 ± 0.02	3.65 ± 0.11	1.79	15.38 ± 0.0	16.7 ± 0.0	2.8 ± 0.0	6.78
1422 + 580	1.52	0.683	N	18.38	1.2/28	18.35 ± 0.05	> 22.00	18.38 ± 0.06	> 22.3
1424 + 240	1.10	...	N	15.45	2.3/139	14.66 ± 0.01	> 21.00	14.75 ± 0.03	> 18.3
1426 + 428	0.70	0.129	E	15.98	490/145	17.38 ± 0.20	16.14 ± 0.01	2.25 ± 0.08	1.95	15.98 ± 0.0	16.84 ± 0.0	2.2 ± 0.0	11.9
1437 + 398	1.10	...	E	16.82	103/113	16.73 ± 0.07	17.95 ± 0.02	1.80 ± 0.05	1.50	16.48 ± 0.0	18.6 ± 0.0	1.6 ± 0.0	12.1
1440 + 122	0.74	0.162	E	16.60	190/106	16.93 ± 0.12	16.71 ± 0.02	3.90 ± 0.25	2.86	16.98 ± 0.0	17.36 ± 0.0	2.1 ± 0.0	7.16
1458 + 224	0.86	0.235	U	15.83	25/97	15.78 ± 0.08	17.80 ± 0.05	3.2 ± 0.8	1.74	15.58 ± 0.1	18.6 ± 0.1	2.40 ± 0.3	1.89
1514 − 241	0.63	0.049	E	13.92	1000/290	14.48 ± 0.12	14.45 ± 0.01	3.70 ± 0.10	3.96	13.58 ± 0.0	15.17 ± 0.0	5.10 ± 0.0	7.67
1517 + 656	1.10	> 0.7	N	16.51	4.6/87	16.18 ± 0.03	> 19.89	18.93 ± 0.05	> 20.5
1519 − 273	1.10	...	N	16.88	1.3/121	17.03 ± 0.04	> 20.40	17.08 ± 0.04	> 21.2
1533 + 535	1.10	* 0.89	N	17.77	3.0/94	17.88 ± 0.05	> 19.70	17.78 ± 0.05	> 20.7
1534 + 014	1.04	0.312	E	17.81	130/114	19.08 ± 0.15	18.16 ± 0.02	2.00 ± 0.10	3.14	17.88 ± 0.0	18.76 ± 0.0	1.80 ± 0.0	13.0
1538 + 149	1.51	0.605	U	17.70	3.4/50	17.94 ± 0.05	20.22 ± 0.40	2.5 ± 1.2	1.98	17.89 ± 0.05	21.08 ± 0.25	1.5 ± 0.5	1.86
1544 + 820	1.10	...	N	16.46	1.7/99	16.55 ± 0.04	> 19.60	16.58 ± 0.04	> 20.0
1553 + 113	1.10	...	N	15.34	2.35/149	14.43 ± 0.01	> 21.60	14.41 ± 0.01	> 22.3
1704 + 604	0.96	0.280	E	18.49	190/63	21.08 ± 0.35	18.69 ± 0.01	0.85 ± 0.03	3.18	19.18 ± 0.10	19.29 ± 0.02	0.9 ± 0.1	9.50
1722 + 119	1.10	...	N	15.11	1.6/133	14.61 ± 0.00	> 21.40	14.61 ± 0.0	> 22.1
1728 + 502	0.64	0.055	E	15.15	400/244	16.43 ± 0.10	15.49 ± 0.02	3.15 ± 0.05	4.35	15.28 ± 0.0	16.02 ± 0.0	3.1 ± 0.0	11.3
1738 + 476	1.05	...	N	19.49	7.2/25	19.63 ± 0.04	> 20.50	19.53 ± 0.07	> 21.2
1745 + 504	1.10	...	E	19.23	490/68	21.18 ± 0.20	19.57 ± 0.02	0.30 ± 0.10	4.14	19.78 ± 0.0	20.1 ± 0.0	1.0 ± 0.0	105
1749 + 096	1.06	0.320	U	16.91	8.5/73	16.88 ± 0.05	18.82 ± 0.10	3.0 ± 0.80	1.39	17.13 ± 0.05	19.62 ± 0.05	2.20 ± 0.20	1.23
1749 + 701	1.46	0.770	N	15.71	1.86/114	15.83 ± 0.04	> 19.28	15.78 ± 0.04	> 20.08
1757 + 703	1.26	0.407	E	18.22	4.85/32	18.43 ± 0.14	19.58 ± 0.25	0.85 ± 0.50	3.72	17.68 ± 0.01	20.38 ± 0.10	2.55 ± 0.33	1.87
1803 + 784	1.50	0.684	N	16.05	1.35/83	16.18 ± 0.02	> 20.89	16.18 ± 0.04	> 20.99
1807 + 698	0.64	0.051	E	14.29	1560/151	14.95 ± 0.25	13.87 ± 0.02	2.10 ± 0.10	1.79	13.85 ± 0.25	14.40 ± 0.05	2.40 ± 0.0	2.43
1823 + 568	1.51	0.664	U	18.02	2.5/52	18.29 ± 0.10	20.24 ± 0.30	0.60 ± 0.2	1.02	18.18 ± 0.05	21.14 ± 0.25	0.80 ± 0.15	1.24
1853 + 671	0.82	0.212	E	17.96	200/78	19.48 ± 0.10	18.19 ± 0.01	1.50 ± 0.08	1.85	18.58 ± 0.0	18.79 ± 0.0	1.1 ± 0.0	6.45
1914 − 194	1.10	...	U	15.81	12/104	15.30 ± 0.03	16.95 ± 0.05	7.40 ± 0.85	3.02	15.28 ± 0.04	17.92 ± 0.02	3.00 ± 0.15	3.57
1959 + 650	0.63	0.048	E	14.59	400/251	15.38 ± 0.10	14.92 ± 0.02	5.10 ± 0.10	3.86	14.58 ± 0.0	15.52 ± 0.0	4.40 ± 0.0	6.16
2005 − 489	0.65	0.071	E	13.61	900/301	12.73 ± 0.01	14.52 ± 0.01	5.65 ± 0.08	7.69	12.58 ± 0.0	15.12 ± 0.0	5.0 ± 0.0	26.4

Table 3—Continued

Object	(V-R) (b)	z (c)	Host (d)	m _R (e)	χ _ν ² /pnt (f)	de Vaucouleurs law fit				Disk galaxy fit			
						m _R point (g)	m _R host (h)	r _e (i)	χ _ν ² (f)	m _R point (g)	m _R host (h)	r _e (i)	χ _ν ²
2007 + 777	1.11	0.342	U	18.02	10/59	18.03 ± 0.10	19.03 ± 0.10	3.3 ± 0.9	1.30	17.78 ± 0.05	19.88 ± 0.05	1.80 ± 0.15	1.92
2037 + 521	1.10	...	E	16.33	3000/151	19.48 ± 0.30	16.15 ± 0.10	4.60 ± 0.25	1.48	18.18 ± 0.0	16.75 ± 0.0	2.8 ± 0.0	16.1
2131 - 021	1.49	1.285	N	18.87	1.6/26	19.00 ± 0.05	> 21.98	19.23 ± 0.05	> 23.6
2143 + 070	0.86	0.237	E	17.40	50/101	18.21 ± 0.11	17.89 ± 0.02	2.10 ± 0.15	1.48	17.59 ± 0.04	18.57 ± 0.03	1.80 ± 0.05	2.74
2149 + 173	1.10	...	N	18.36	1.7/51	18.63 ± 0.06	> 21.60	18.6 ± 0.05	> 22.2
2200 + 420	0.61	0.069	E	14.11	42.3/179	13.58 ± 0.05	15.55 ± 0.02	4.8 ± 0.04	0.90	13.30 ± 0.01	16.64 ± 0.01	4.20 ± 0.01	1.74
2201 + 044	0.63	0.027	E	14.07	247/223	17.18 ± 0.05	13.74 ± 0.01	6.78 ± 0.08	1.03	17.2 ± 0.0	14.37 ± 0.0	3.0 ± 0.0	110
2240 - 260	1.45	* 0.774	N	17.28	1.5/61	17.53 ± 0.02	> 22.08	17.48 ± 0.02	> 22.8
2254 + 074	0.78	0.190	E	16.17	96/172	16.94 ± 0.12	16.61 ± 0.02	4.90 ± 0.35	2.45	16.54 ± 0.0	17.17 ± 0.01	3.7 ± 0.05	2.97
2326 + 174	0.82	0.213	E	17.08	160/102	17.63 ± 0.11	17.56 ± 0.03	1.80 ± 0.15	1.50	16.93 ± 0.0	18.24 ± 0.0	1.6 ± 0.0	4.06
2344 + 514	0.63	0.044	E	14.30	5000/199	16.83 ± 0.05	14.01 ± 0.01	5.93 ± 0.02	3.03	15.08 ± 0.0	14.62 ± 0.0	4.0 ± 0.0	89.8
2356 - 309	0.74	0.165	E	16.51	120/119	17.28 ± 0.13	17.21 ± 0.02	1.85 ± 0.10	1.36	16.43 ± 0.05	17.91 ± 0.02	1.80 ± 0.05	2.15

(a) All magnitudes refer to the Cousins R band, including sources observed with filters F606W and F555W.

(b) Adopted host galaxy color used to convert magnitudes from WFPC2 filters to Cousins R (interpolated from values in Fukugita et al. 1995). For the point source $(V - R) = 0.3$ mag was adopted, as appropriate for a power law spectrum with spectral index -1 .

(c) Reported redshift for the BL Lac object. Most HBL redshifts were determined from weak stellar absorption features arising in the BL Lac host galaxy; LBL redshifts were more often derived from (weak) emission lines, in some cases a single line. Particularly uncertain values are indicated with asterisks (*); for details, see the Appendix.

(d) Code for galaxy detection and morphology class. N = host not resolved, U = host resolved but morphologically unclassified, E=elliptical, D = disk.

(e) Observed total magnitude integrated to the last useful point of the radial profile as shown in Figure 1. This magnitude is independent of the fit. Note that this value can not be obtained simply combining the magnitudes of the two best fit components (next columns) because different color transformations apply to each component, and the host magnitude is extrapolated to infinity.

(f) Reduced best-fit χ^2 obtained fitting the PSF alone, and number of data points used to describe the average radial profile.

(g) Best-fit R-band magnitude of point source. Errors in this and following columns are 68% confidence statistical uncertainties as derived from χ^2 distribution. Systematic errors, typically several tenths of a magnitude, actually dominate.

(h) Best-fit R-band magnitude of host galaxy, extrapolated to infinity. Upper limits are 99% confidence, evaluated assuming $r_e = 10$ kpc.

(i) Best-fit effective (half-light) radius in arcsec.

(l) Best fit reduced χ^2 for the PSF+galaxy model.

Fig. 1.— **Figure 1.** For each BL Lac object up to four panels are shown. The top panel is the final combined, cosmic-ray-cleaned image in gray scale. The next panel is a contour plot of the same image, which better reveals a large range in surface brightness. Contours start at the surface brightness (in mag arcsec⁻²) indicated at the bottom of each figure and are separated by 0.5 magnitudes. The two upper panels have the same size and orientation, which are reported on the contour panel; north and east are marked. The third panel shows the average surface brightness radial profile (*filled squares*), and the best-fit PSF plus de Vaucouleurs model (or only the PSF for unresolved sources). *Dotted line*: the PSF model. *Dashed line*: de Vaucouleurs model convolved with the PSF. *Solid line*: sum of the two components. When not visible, the dashed line is superimposed on the solid line. In several images the central point source is saturated (sometimes heavily). Saturation shows up usually in the first 2 or 3 pixels of the radial profile, either as a flat plateau (e.g., 1914-194), or as a region of decreasing flux (e.g., 1144-379). In some other cases the saturation was not that heavy and the software was able to recover partially the true nuclear brightness by combining long and short (unsaturated) images; the radial profile then shows a modest, less-than-proportional increase of flux going toward the center (e.g., 1044+549 and 1407+595). For comparison, two cases of unsaturated radial profiles are 1426+428 and 1440+122. For the three exceptional objects 0145+138, 0446+449, and 0525+713, which have no detectable point source, we fitted the radial profile with a galaxy model only. For 0446+449 the profile is a perfect exponential, the only case of a disk galaxy in the entire sample (and one with no bright nucleus). For resolved BL Lacs, a fourth panel shows the χ^2 contours for the two parameters of interest in the PSF-plus-de Vaucouleurs fit, r_e and m_R , with best-fit values marked by a square. The contours represent 68%, 95%, 99% probabilities.

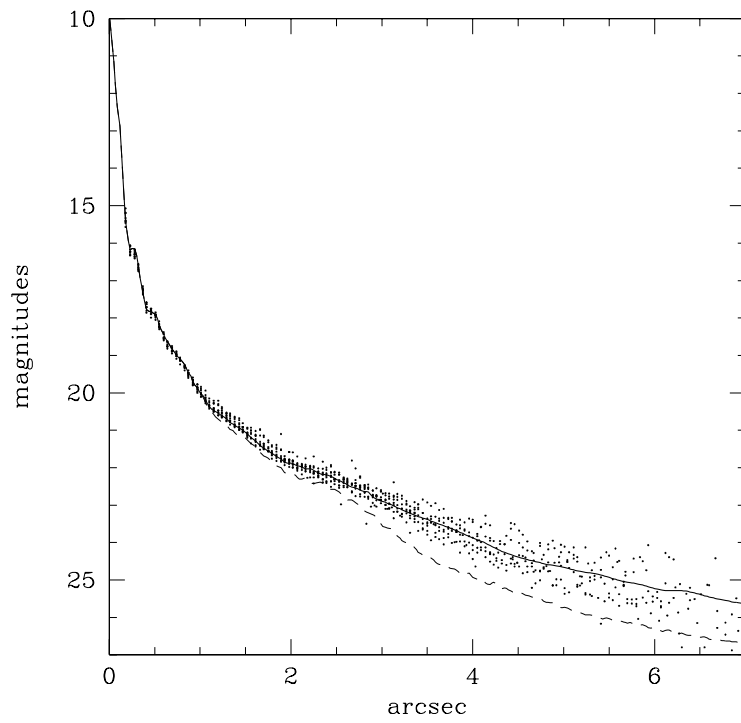


Fig. 2.— **Figure 2.** Radial profile derived from several bright stars (dots), compared with the Tiny Tim-generated PSF (*dashed line*) and our composite PSF model (*solid line*).

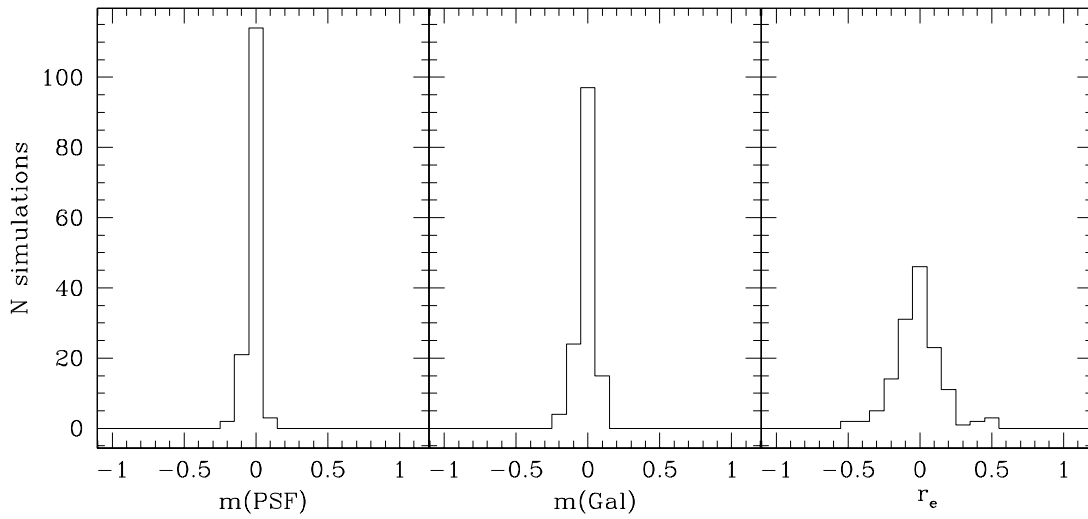


Fig. 3.— **Figure 3.** The distribution of best-fit minus input values of nuclear apparent magnitude, host galaxy apparent magnitude, and effective radius (in arcseconds) for simulated *HST* images, analyzed according to our standard procedures. The mean values are centered at zero and the dispersions are within our estimated statistical errors, meaning we recover the true value with no systematic deviations and with high accuracy. In the simulations, nuclear magnitudes were varied from 15 to 18 mag, the host magnitudes from 15 to 21 mag, and the effective radii from 0.8 to 5 arcsec, which represent the values most often observed in our data.

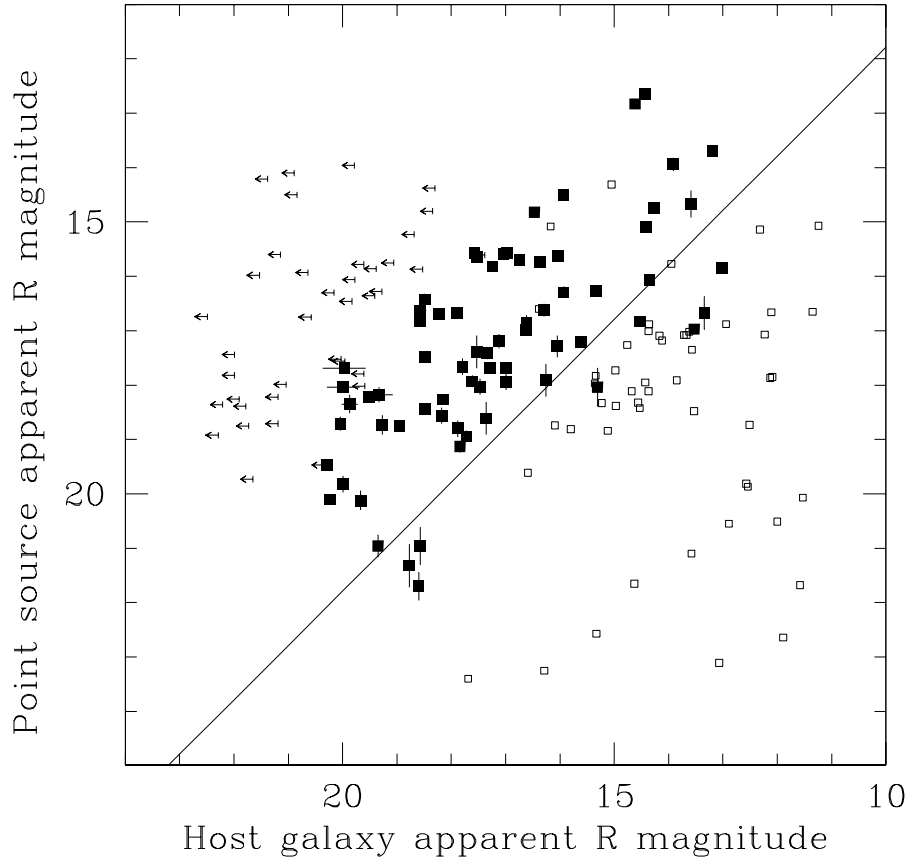


Fig. 4.— **Figure 4.** Host galaxy versus nuclear magnitude for all 110 BL Lac objects (*solid squares represent resolved sources, while arrows are upper limits for unresolved objects*). The solid line is the locus for an elliptical galaxy with a nuclear luminosity that reduces an intrinsic 50% 4000Å break to 25%, the usual distinction between a BL Lac object and a radio galaxy. The nuclear non-thermal component is assumed to have spectral index $\alpha = -1.5$, which includes all but the steepest BL Lacs. Objects with flatter spectral indices would be located to the left of this line. Objects above the line have bright nuclei compared to their host galaxies and are classified as BL Lacs. Below the line the light from the galaxy dominates and the source is classified as radio galaxy. Sources can cross the limit because of nuclear flux variability. Radio galaxies (*open squares; Govoni et al. 1999, Chiaberge et al. 1999*) smoothly fill the lower half of the diagram, showing that the distinction from BL Lac objects occurs at an arbitrary point.

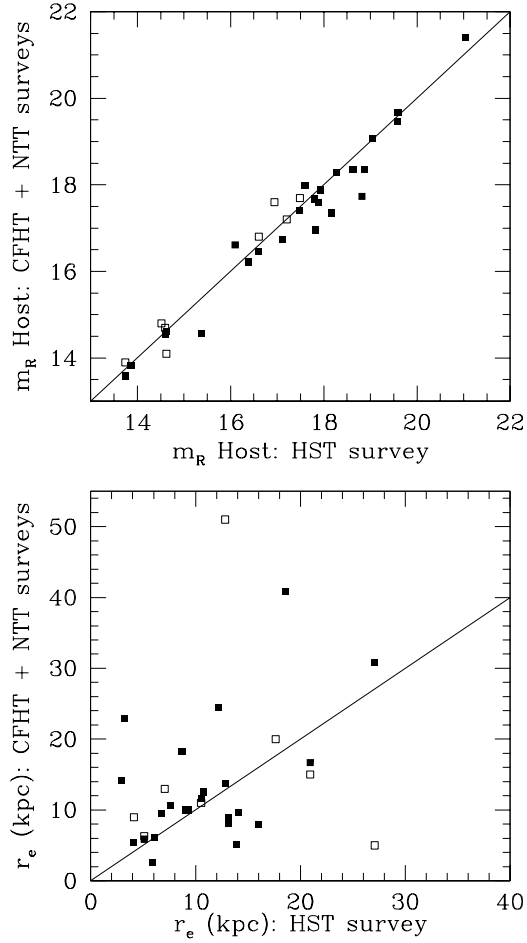


Fig. 5.— **Figure 5.** Comparison of our *HST* results with those from two large ground-based surveys. *Filled squares*: Canada-France-Hawaii-Telescope survey (Wurtz, Stocke & Yee 1996). *Open squares*: ESO-NTT survey (Falomo 1996). The magnitudes agree well, with an average difference of 0.1 mag and an rms dispersion of 0.4 mag. The scatter in measured radius is much larger.

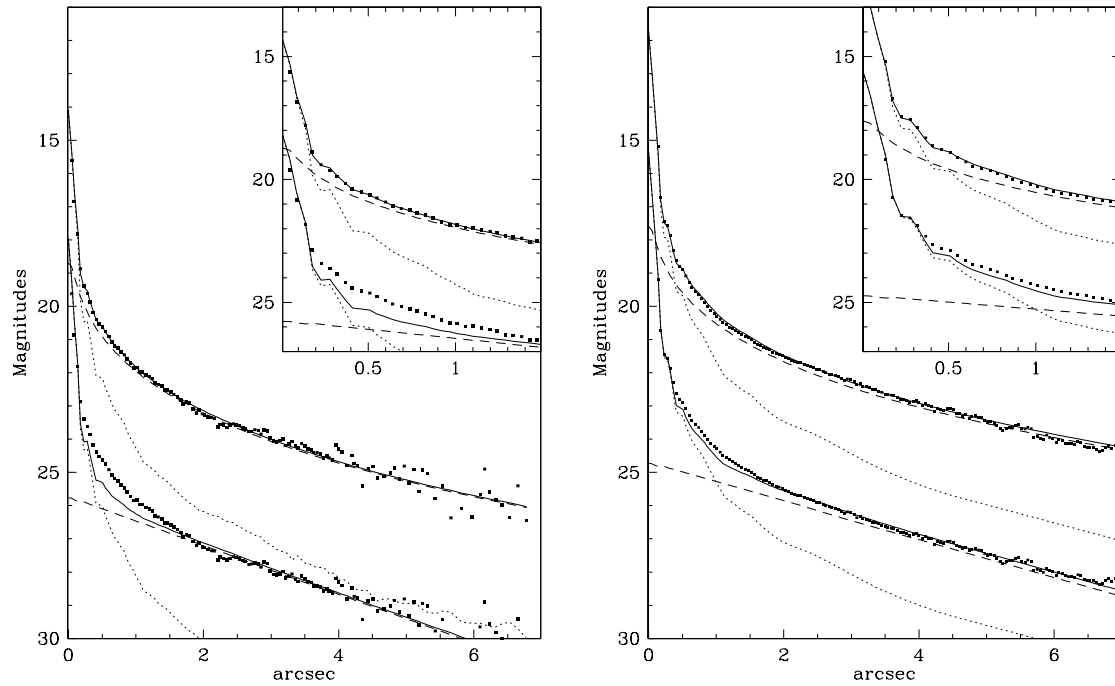


Fig. 6.— **Figure 6.** Comparison of the best de Vaucouleurs and disk fits for two illustrative sources, 0607+710 (*left*) and 1418+546 (*right*). To compare the two, the disk fit is shifted downward by 4 mag. The inset shows an enlargement of the central portion of the radial profile. The PSF is shown as a dotted line, the galaxy as a dashed line, and the sum of the two components as a solid line. In both cases, the exponential disk fails by a small but highly significant amount to reproduce the observed light in the central 1.5 arcsec, which is the case for most of the BL Lac host galaxies.

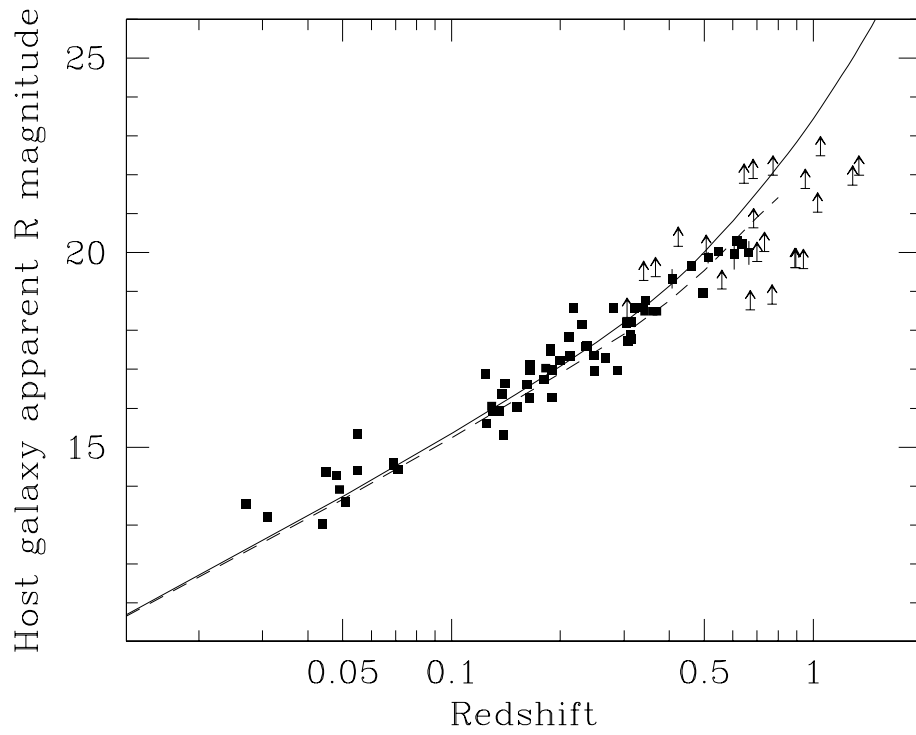


Fig. 7.— **Figure 7.** Hubble diagram for BL Lac host galaxies. The solid line is for an object of absolute magnitude $M_R = -23.7$ mag, while the dashed line is for the same object including passive evolution (Bressan *et al.* 1994). The data (*filled squares*) are consistent with either line, with few resolved host galaxies at $z \gtrsim 0.6$.

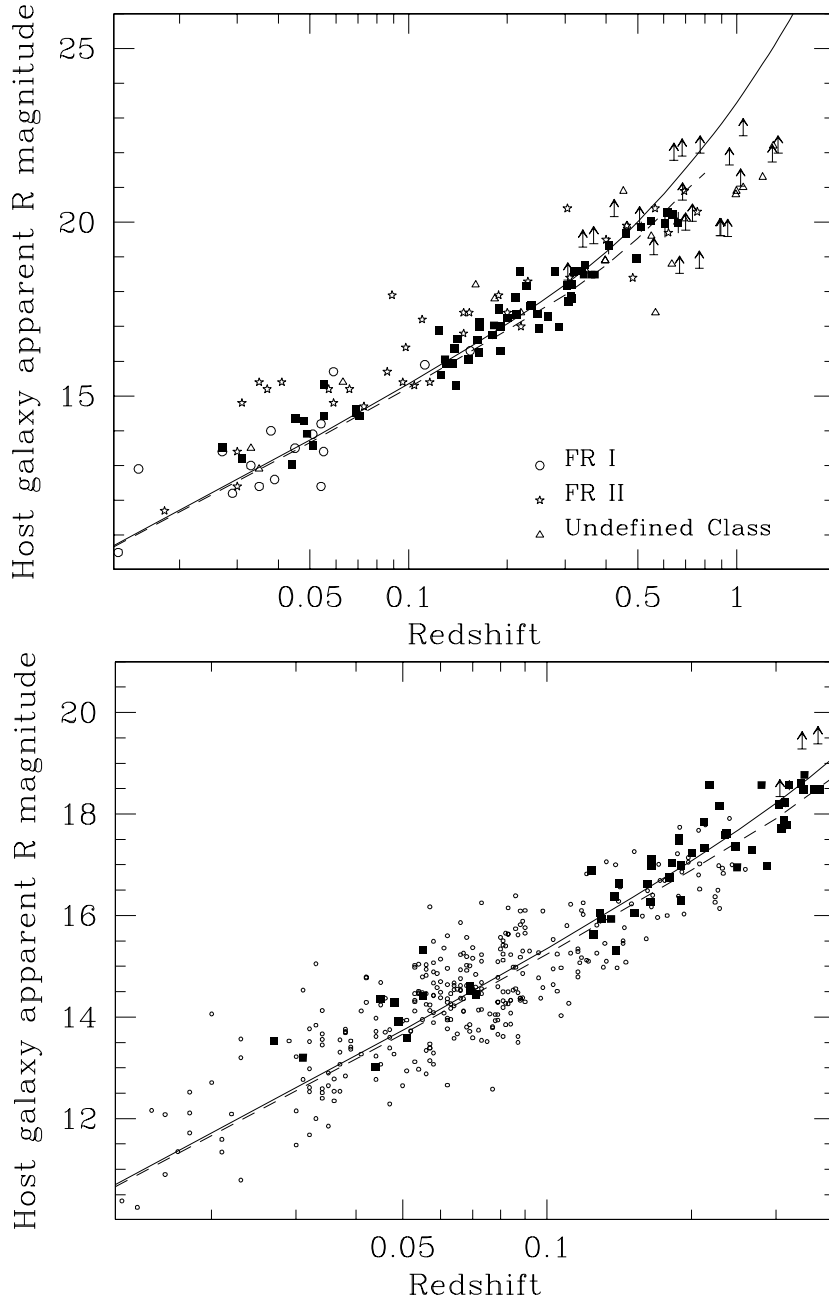


Fig. 8.— **Figure 8.** Hubble diagram for BL Lac host galaxies and radio galaxies. *Upper panel:* BL Lacs (solid squares) are compared with radio galaxies from the 2 Jy sample (open symbols; Morganti *et al.* 1993). *Lower panel:* The low-redshift region from the previous panel, with radio galaxy data (dots) from Ledlow & Owen (1995) and Govoni *et al.* (1999).

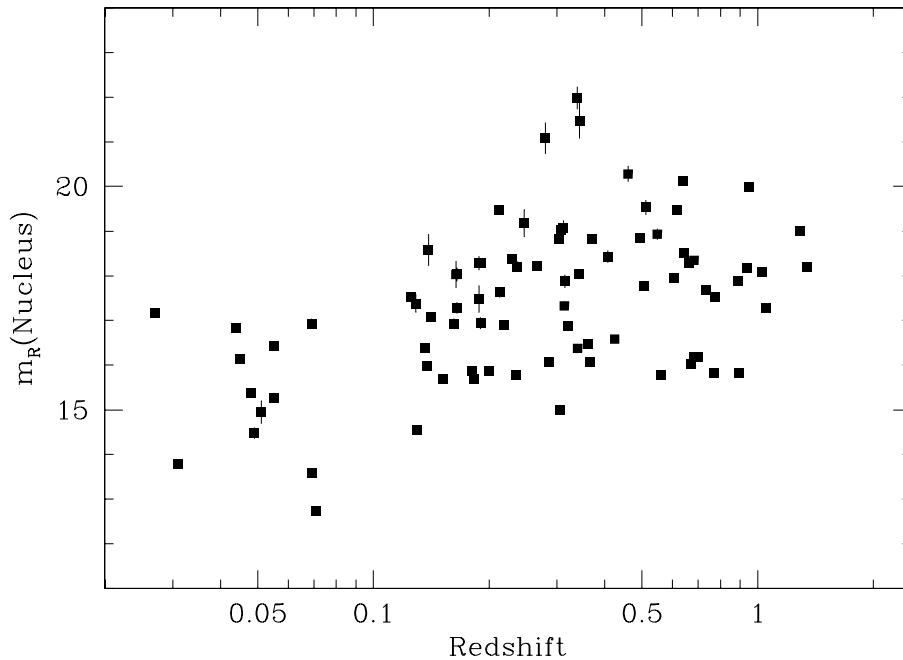


Fig. 9.— **Figure 9.** Apparent R magnitude of the nuclear component, as a function of redshift. All sources except 0145+138, 0446+449, and 0525+713, which have no central point sources, are shown. For resolved sources the best-fit point source magnitude is plotted, as derived from a PSF plus de Vaucouleurs model even when the host remains morphologically unclassified. Few of the nuclei are fainter than $m_R \sim 20$ mag because of the effective flux limit imposed by optical identification of radio or X-ray samples. In strong contrast to the Hubble diagram for the host galaxies, the apparent magnitude of the nuclear component does not vary strongly with distance, as expected in flux-limited samples, for which luminosity increases with redshift. The shallow envelope in the lower right reflects the luminosity function, while the upper left would be populated by radio galaxies.

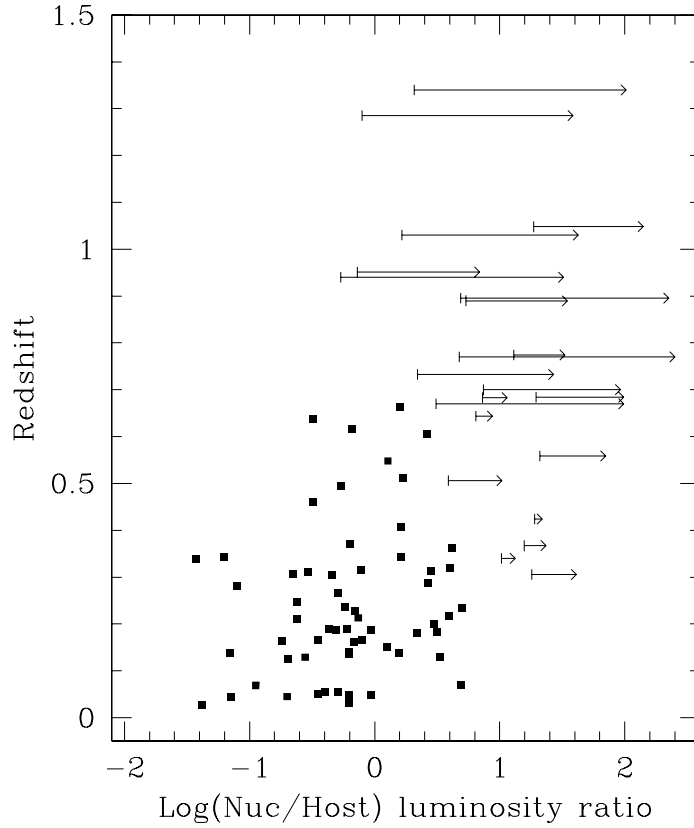


Fig. 10.— **Figure 10.** The L_{nuc}/L_{host} luminosity ratio as a function of distance, using K-corrected data. For unresolved objects, we plot a range of ratios (*horizontal arrows*). The minimum ratio (leftmost extreme of the arrow) corresponds to the upper limit to the host galaxy magnitude. The maximum ratio (rightmost extreme) is the ratio assuming a galaxy luminosity $M_R = -22.8$ mag (1 mag fainter than the average of the sample). The ratio of nucleus to host galaxy luminosity increases with redshift, as the point source luminosity increases.

This figure "fig1a.gif" is available in "gif" format from:

<http://arxiv.org/ps/astro-ph/9911147v1>

This figure "fig1aa.gif" is available in "gif" format from:

<http://arxiv.org/ps/astro-ph/9911147v1>

This figure "fig1ab.gif" is available in "gif" format from:

<http://arxiv.org/ps/astro-ph/9911147v1>

This figure "fig1ac.gif" is available in "gif" format from:

<http://arxiv.org/ps/astro-ph/9911147v1>

This figure "fig1ad.gif" is available in "gif" format from:

<http://arxiv.org/ps/astro-ph/9911147v1>

This figure "fig1ae.gif" is available in "gif" format from:

<http://arxiv.org/ps/astro-ph/9911147v1>

This figure "fig1af.gif" is available in "gif" format from:

<http://arxiv.org/ps/astro-ph/9911147v1>

This figure "fig1ag.gif" is available in "gif" format from:

<http://arxiv.org/ps/astro-ph/9911147v1>

This figure "fig1ah.gif" is available in "gif" format from:

<http://arxiv.org/ps/astro-ph/9911147v1>

This figure "fig1ai.gif" is available in "gif" format from:

<http://arxiv.org/ps/astro-ph/9911147v1>

This figure "fig1aj.gif" is available in "gif" format from:

<http://arxiv.org/ps/astro-ph/9911147v1>

This figure "fig1ak.gif" is available in "gif" format from:

<http://arxiv.org/ps/astro-ph/9911147v1>

This figure "fig1a.gif" is available in "gif" format from:

<http://arxiv.org/ps/astro-ph/9911147v1>

This figure "fig1am.gif" is available in "gif" format from:

<http://arxiv.org/ps/astro-ph/9911147v1>

This figure "fig1an.gif" is available in "gif" format from:

<http://arxiv.org/ps/astro-ph/9911147v1>

This figure "fig1ao.gif" is available in "gif" format from:

<http://arxiv.org/ps/astro-ph/9911147v1>

This figure "fig1ap.gif" is available in "gif" format from:

<http://arxiv.org/ps/astro-ph/9911147v1>

This figure "fig1aq.gif" is available in "gif" format from:

<http://arxiv.org/ps/astro-ph/9911147v1>

This figure "fig1ar.gif" is available in "gif" format from:

<http://arxiv.org/ps/astro-ph/9911147v1>

This figure "fig1as.gif" is available in "gif" format from:

<http://arxiv.org/ps/astro-ph/9911147v1>

This figure "fig1at.gif" is available in "gif" format from:

<http://arxiv.org/ps/astro-ph/9911147v1>

This figure "fig1au.gif" is available in "gif" format from:

<http://arxiv.org/ps/astro-ph/9911147v1>

This figure "fig1av.gif" is available in "gif" format from:

<http://arxiv.org/ps/astro-ph/9911147v1>

This figure "fig1aw.gif" is available in "gif" format from:

<http://arxiv.org/ps/astro-ph/9911147v1>

This figure "fig1ax.gif" is available in "gif" format from:

<http://arxiv.org/ps/astro-ph/9911147v1>

This figure "fig1ay.gif" is available in "gif" format from:

<http://arxiv.org/ps/astro-ph/9911147v1>

This figure "fig1az.gif" is available in "gif" format from:

<http://arxiv.org/ps/astro-ph/9911147v1>

This figure "fig1b.gif" is available in "gif" format from:

<http://arxiv.org/ps/astro-ph/9911147v1>

This figure "fig1ba.gif" is available in "gif" format from:

<http://arxiv.org/ps/astro-ph/9911147v1>

This figure "fig1bb.gif" is available in "gif" format from:

<http://arxiv.org/ps/astro-ph/9911147v1>

This figure "fig1bc.gif" is available in "gif" format from:

<http://arxiv.org/ps/astro-ph/9911147v1>

This figure "fig1c.gif" is available in "gif" format from:

<http://arxiv.org/ps/astro-ph/9911147v1>

This figure "fig1d.gif" is available in "gif" format from:

<http://arxiv.org/ps/astro-ph/9911147v1>

This figure "fig1e.gif" is available in "gif" format from:

<http://arxiv.org/ps/astro-ph/9911147v1>

This figure "fig1f.gif" is available in "gif" format from:

<http://arxiv.org/ps/astro-ph/9911147v1>

This figure "fig1g.gif" is available in "gif" format from:

<http://arxiv.org/ps/astro-ph/9911147v1>

This figure "fig1h.gif" is available in "gif" format from:

<http://arxiv.org/ps/astro-ph/9911147v1>

This figure "fig1i.gif" is available in "gif" format from:

<http://arxiv.org/ps/astro-ph/9911147v1>

This figure "fig1j.gif" is available in "gif" format from:

<http://arxiv.org/ps/astro-ph/9911147v1>

This figure "fig1k.gif" is available in "gif" format from:

<http://arxiv.org/ps/astro-ph/9911147v1>

This figure "fig11.gif" is available in "gif" format from:

<http://arxiv.org/ps/astro-ph/9911147v1>

This figure "fig1m.gif" is available in "gif" format from:

<http://arxiv.org/ps/astro-ph/9911147v1>

This figure "fig1n.gif" is available in "gif" format from:

<http://arxiv.org/ps/astro-ph/9911147v1>

This figure "fig1o.gif" is available in "gif" format from:

<http://arxiv.org/ps/astro-ph/9911147v1>

This figure "fig1p.gif" is available in "gif" format from:

<http://arxiv.org/ps/astro-ph/9911147v1>

This figure "fig1q.gif" is available in "gif" format from:

<http://arxiv.org/ps/astro-ph/9911147v1>

This figure "fig1r.gif" is available in "gif" format from:

<http://arxiv.org/ps/astro-ph/9911147v1>

This figure "fig1s.gif" is available in "gif" format from:

<http://arxiv.org/ps/astro-ph/9911147v1>

This figure "fig1t.gif" is available in "gif" format from:

<http://arxiv.org/ps/astro-ph/9911147v1>

This figure "fig1u.gif" is available in "gif" format from:

<http://arxiv.org/ps/astro-ph/9911147v1>

This figure "fig1v.gif" is available in "gif" format from:

<http://arxiv.org/ps/astro-ph/9911147v1>

This figure "fig1w.gif" is available in "gif" format from:

<http://arxiv.org/ps/astro-ph/9911147v1>

This figure "fig1x.gif" is available in "gif" format from:

<http://arxiv.org/ps/astro-ph/9911147v1>

This figure "fig1y.gif" is available in "gif" format from:

<http://arxiv.org/ps/astro-ph/9911147v1>

This figure "fig1z.gif" is available in "gif" format from:

<http://arxiv.org/ps/astro-ph/9911147v1>